OXFORD

Human Molecular Genetics, 2016, Vol. 25, No. 22 4920–4938

doi: 10.1093/hmg/ddw316
Advance Access Publication Date: 16 September 2016
Original Article

ORIGINAL ARTICLE

A small molecule p75^{NTR} ligand normalizes signalling and reduces Huntington's disease phenotypes in R6/2 and BACHD mice

Danielle A. Simmons[1,*], Nadia P. Belichenko[1], Ellen C. Ford[1], Sarah Semaan[1], Marie Monbureau[2], Sruti Aiyaswamy[1], Cameron M. Holman[1], Christina Condon[1], Mehrdad Shamloo[2,3], Stephen M. Massa[4] and Frank M. Longo[1]

[1]Department of Neurology and Neurological Sciences, Stanford University School of Medicine, [2]Behavioral and Functional Neuroscience Laboratory, Institute for Neuro-Innovation and Translational Neurosciences, [3]Department of Neurosurgery, Stanford University School of Medicine, Stanford, CA, USA and [4]Department of Neurology and Laboratory for Computational Neurochemistry and Drug Discovery, Department of Veterans Affairs Medical Center and Department of Neurology, University of California–San Francisco, San Francisco, CA, USA

*To whom correspondence should be addressed at: Danielle A. Simmons, 1201 Welch Rd., MSLS P252, Stanford, CA 94305, USA. Tel: 650-736-0770; Fax: 650-498-4579; Email: simmons3@stanford.edu

Abstract

Decreases in the ratio of neurotrophic versus neurodegenerative signalling play a critical role in Huntington's disease (HD) pathogenesis and recent evidence suggests that the p75 neurotrophin receptor (NTR) contributes significantly to disease progression. p75^{NTR} signalling intermediates substantially overlap with those promoting neuronal survival and synapse integrity and with those affected by the mutant huntingtin (muHtt) protein. MuHtt increases p75^{NTR}-associated deleterious signalling and decreases survival signalling suggesting that p75^{NTR} could be a valuable therapeutic target. This hypothesis was investigated by examining the effects of an orally bioavailable, small molecule p75^{NTR} ligand, LM11A-31, on HD-related neuropathology in HD mouse models (R6/2, BACHD). LM11A-31 restored striatal AKT and other pro-survival signalling while inhibiting c-Jun kinase (JNK) and other degenerative signalling. Normalizing p75^{NTR} signalling with LM11A-31 was accompanied by reduced Htt aggregates and striatal cholinergic interneuron degeneration as well as extended survival in R6/2 mice. The p75^{NTR} ligand also decreased inflammation, increased striatal and hippocampal dendritic spine density, and improved motor performance and cognition in R6/2 and BACHD mice. These results support small molecule modulation of p75^{NTR} as an effective HD therapeutic strategy. LM11A-31 has successfully completed Phase I safety and pharmacokinetic clinical trials and is therefore a viable candidate for clinical studies in HD.

Received: June 8, 2016. **Revised:** August 18, 2016. **Accepted:** September 12, 2016

Introduction

Huntington's disease (HD) is a neurodegenerative disorder characterized by motor, cognitive and psychiatric disturbances arising from preferential damage to medium spiny neurons (MSNs) in the striatum as well as cortical and hippocampal neurodegeneration (1,2). The disease is caused by a mutation that extends the trinucleotide CAG repeat region in exon 1 of the *HTT* gene generating a mutant huntingtin (muHtt) protein with a polyglutamine expansion (3). MuHtt reduces neurotrophic support, largely due to deficient brain-derived neurotrophic factor (BDNF) signalling via its tropomyosin receptor kinase B (TrkB) receptor, and this deficit is thought to have a prominent causal role in developing fundamental HD pathologies (4,5).

Neurotrophins (NTs) bind to specific Trk receptors and with lower affinity to the 75 kDa pan-NT receptor ($p75^{NTR}$) (6,7). $p75^{NTR}$ lacks intrinsic catalytic activity but has the ability to regulate diverse cellular processes including active cell death via recruitment of intracellular adaptor proteins and modulation of other receptors. NT-$p75^{NTR}$ binding can potentiate Trk function and thereby promote trophic signalling, depending on the cellular context and Trk abundance, and can activate degenerative pathways with a co-receptor sortilin, which is up-regulated in HD, and may also independently promote survival or degenerative signalling (8–11). Lack of NTs leads to a 'dependence receptor' mode of $p75^{NTR}$ signalling that activates degenerative pathways (7). States in which an NT and/or Trk deficiency exist along with increased $p75^{NTR}$ expression may be particularly deleterious (12–14). This state occurs in HD patients and multiple HD mouse models, wherein $p75^{NTR}$ levels are increased in striatum and hippocampus and TrkB levels and/or downstream signalling are decreased (12,15–18). This imbalance contributes to altered $p75^{NTR}$ signalling which impairs TrkB signalling and negatively impacts structural and functional synaptic plasticity in HD mouse models (12,15,17,19). $p75^{NTR}$ signalling intermediates overlap many of those that are responsible for neuronal survival and synapse integrity as well as those affected by muHtt and/or other HD-related mechanisms (*e.g.* excitotoxicity, inflammation; Fig. 1) (7,12,19,20). Pharmacological and/or genetic inhibition of some of these signalling intermediates restored BDNF-dependent long-term potentiation (LTP) in indirect pathway spiny projection neurons in striatum of the BACHD mouse model of HD (17). Normalizing hippocampal $p75^{NTR}$ expression via genetic means or treatment with fingolimod, a sphingosine-1 phosphate receptor modulator, reduced degenerative signalling and restored both structural and functional aspects of synaptic plasticity and memory in HD mouse models (15,19). These studies strongly suggest $p75^{NTR}$ as a viable HD therapeutic target especially if its pro-survival signalling can be activated while its deleterious signalling is inhibited.

The hypothesis that a $p75^{NTR}$ ligand may inhibit degeneration and promote neuronal function in HD through interactions with the many signalling pathways affected by muHtt (as in Fig. 1) was tested directly in this study using a small molecule $p75^{NTR}$ ligand, LM11A-31. LM11A-31 binds to $p75^{NTR}$ and not Trk receptors, down-regulates $p75^{NTR}$-related degenerative signalling, up-regulates trophic signalling (21–23) and prevents neurodegeneration in *in vitro* studies (23–28) and animal models of multiple neurological disease states (29–31), including post-traumatic brain injury and Alzheimer's disease (30,32–34). Here we report that oral administration of LM11A-31 to two HD mouse models normalizes $p75^{NTR}$ signalling, reduces key HD neuropathologies, including Htt aggregation and dendritic spine loss, and improves cognition and motor performance, providing evidence that targeting $p75^{NTR}$ may be an effective strategy for the treatment of HD.

Results

LM11A-31 decreases $p75^{NTR}$-associated degenerative signalling and increases survival signalling

$p75^{NTR}$ up-regulation and/or TrkB down-regulation in the striatum and hippocampus disrupts neurotrophic support, contributing to reduced survival signalling and augmented degenerative signalling in HD patients and multiple mouse models (11,12,15,19). However, this imbalance had not been previously determined in the R6/2 mouse model of HD. Therefore, levels of full-length $p75^{NTR}$ and TrkB proteins were examined in the striatum of 11-12 week old R6/2 and wild-type (WT) mice treated for 7 weeks with vehicle or LM11A-31. $p75^{NTR}$ levels were increased by 29 ± 8% (mean ± s.e.m) (Fig. 2A) in vehicle-treated R6/2 mice compared to WTs, while TrkB levels were reduced by 20 ± 4.6% (Fig. 2B), as shown previously (18). Consequently, the ratio of $p75^{NTR}$ to TrkB was substantially increased in R6/2 striatum. LM11A-31 did not affect levels of either receptor in either genotype.

NTs and other ligands bind to $p75^{NTR}$ promoting intracellular domain interactions with cell adaptor proteins that regulate downstream signalling and endocytosis. $p75^{NTR}$ differs from most other growth factor receptors in that it is not phosphorylated upon activation and therefore cannot be monitored in this manner to assess target engagement. Ligand binding can induce regulated intramembrane proteolysis which generates a C-terminal fragment (CTF), which is further cleaved to produce an intracellular domain-fragment (ICD) (35–37). It was therefore of interest to determine whether LM11A-31 would promote, inhibit or otherwise modulate $p75^{NTR}$ proteolysis in HD mice, which would also provide an indication of compound function in the brain region of interest. LM11A-31 was previously shown to increase CTF and ICD levels indicating *in vivo* target engagement in an Alzheimer's disease mouse model (33). Thus, to assess *in vivo* target engagement in HD mice and to begin to examine the effects of LM11A-31 on HD-related signalling, the ligand's impact on $p75^{NTR}$ cleavage was assessed. Immunoblotting with an antibody detecting the $p75^{NTR}$ cytoplasmic domain revealed that R6/2-vehicle mice exhibited decreased striatal CTF but not ICD levels relative to WTs (Fig. 2C). Furthermore, LM11A-31 normalized CTF in R6/2 mice and increased ICD levels in both WT and R6/2 mice, demonstrating that the compound promoted $p75^{NTR}$ processing, which indicates that the ligand engaged its intended target (36,38).

MuHtt disrupts multiple signalling pathways intersecting with those regulated by $p75^{NTR}$ (Fig. 1), including c-Jun kinase (JNK), nuclear factor kappa-light-chain-enhancer of activated B cells (NF-κB) and Rho kinase, as well as AKT (6,7,39). Thus, the nature and extent of LM11A-31 effects on key intermediates in these pathways was determined. AKT pathway activation, which is neuroprotective, is reduced in striatum of HD patients and rodent models in advanced disease stages (20,40). Decreased phospho(p)-AKT in the R6/2 striatum was significantly increased by 49 ± 15% (mean ± s.e.m) with LM11A-31 treatment (Fig. 2D). JNK signalling is associated with cell death and is up-regulated by muHtt in striatum of HD rodent models, including R6/2 mice (20,41–43). LM11A-31 prevented JNK activation in R6/2 striatum (Fig. 2E). An inhibitor of kappa beta kinase (IKK)/NFκβ signalling mediates neuroinflammation and,

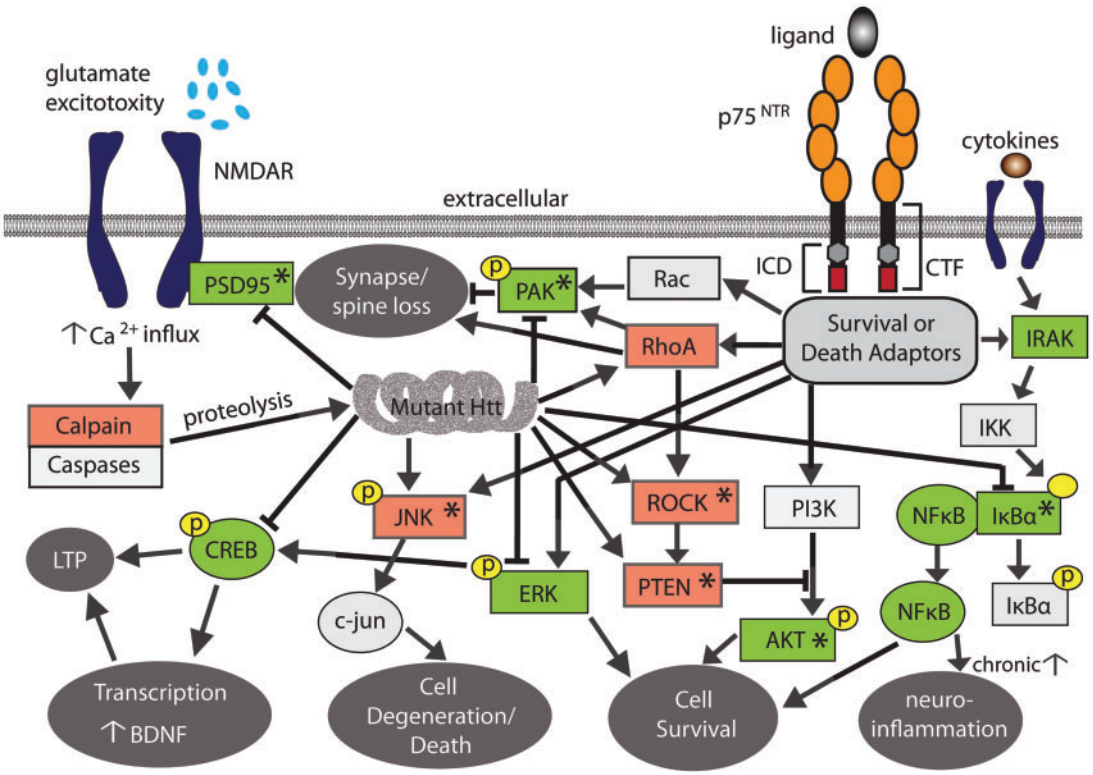

Figure 1. p75^{NTR} signalling pathways and HD neuropathological mechanisms are affected by LM11A-31. Simplified schematic showing the signalling pathways regulated by p75^{NTR} and their overlap with muHtt-affected signalling networks contributing to HD neuropathology. Many signalling pathways regulated by p75^{NTR} are dysregulated by muHtt (arrows indicate up-regulation; ⊢ indicates inhibition). LM11A-31 activates signalling intermediates shown in green while inhibiting those in red as shown previously (23); asterisks indicate intermediates shown to be affected in R6/2 and/or BACHD mice in the present study.

promotes cell survival when regulated (44). However, excessive activation of NFκβ signalling is observed in HD patients and mouse models and contributes to deleterious neuroinflammation (44–46). NFκβ is sequestered by an inhibitor of nuclear factor κB (Iκβα) which prevents it from translocating to the nucleus to activate inflammation-promoting gene expression programs (47–49). Iκβα levels are reduced in the R6/1 hippocampus (15) and, here, are shown to decrease by 29 ± 6% (mean ± s.e.m.) in R6/2 striatum (Fig. 2F), which could cause elevated NFκβ signalling; LM11A-31 mitigated this deficit. The Rho kinase pathway is modulated by p75^{NTR} signalling (50,51) and increased activity/signalling of the small GTPase RhoA has been implicated HD pathogenesis (15,17,19,52–54). p75^{NTR} directly activates RhoA, which activates Rho-associated kinase (ROCK), triggering phosphatase-and-tensin-homolg-deleted-on-chromosome 10 (PTEN) to inhibit phosphoinositide 3-kinase (PI3K) activation of AKT (Fig. 1) (6,51,55,56). ROCK1 levels are increased in brains from HD patients and R6/2 mice (54) and PTEN is increased in inhibitory spiny projection neurons in striatum of BACHD mice (17). In this study, both ROCK1 and PTEN were up-regulated in the R6/2 striatum and these increases were attenuated by LM11A-31 treatment (Fig. 2G and H). Another downstream target of RhoA is p21-activated kinase 1 (PAK1), which, when activated, is neuroprotective and involved in regulating the actin cytoskeleton and neuroplasticity, including LTP consolidation, and increased post-synaptic density (PSD) levels (57–59). R6/2 mice given vehicle had reduced pPAK1 and PSD-95 levels which were normalized by LM11A-31 (Fig. 2I and J).

Striatal levels of p75^{NTR} and the effects of LM11A-31 on its key signalling pathways were also investigated in 9 month-old BACHD mice. Similar to the R6/2 striatum, p75^{NTR} levels are up-regulated in BACHD mice and are unaffected by LM11A-31 treatment (Fig. 2K). It was previously shown that TrkB levels were unaltered in BACHD mice at this age (18). While pAKT levels were similar in striatum of WT and BACHD mice, they were increased in BACHD mice treated with LM11A-31 (Fig. 2L). Both pJNK and PTEN were increased in BACHD-vehicle mice versus WTs, and LM11A-31 significantly reduced pJNK but not PTEN levels (Fig. 2M and N).

LM11A-31 mitigates intranuclear Htt aggregates and striatal DARPP-32 deficits

MuHtt translocates from the cytoplasm to the nucleus of neurons in numerous brain areas of HD patients and mouse models and forms aggregates (60,61). LM11A-31 significantly reduced the number and total area occupied by neuronal intranuclear Htt aggregates in the striatum and cortex but neither of these measures was affected in the hippocampus of 11 week-old R6/2 mice (Fig. 3A–D). In addition, aggregate size was significantly decreased in striatum and hippocampus with LM11A-31 treatment (Fig. 3E).

MuHtt expression decreases striatal volume in HD patients and R6/2 mice (1,61,62), and in this study R6/2 mice showed an 18 ± 3% reduction in striatal volume ($P \leq 0.005$ versus WT-vehicle), which was unaltered by LM11A-31 (Supplementary Material, Fig. S1A). LM11A-31's effects on Htt aggregates and striatal volume were not analysed in BACHD mice as these appear at a more advanced ages [≥12 months; (63,64)] than used in this study [9 months; (18)].

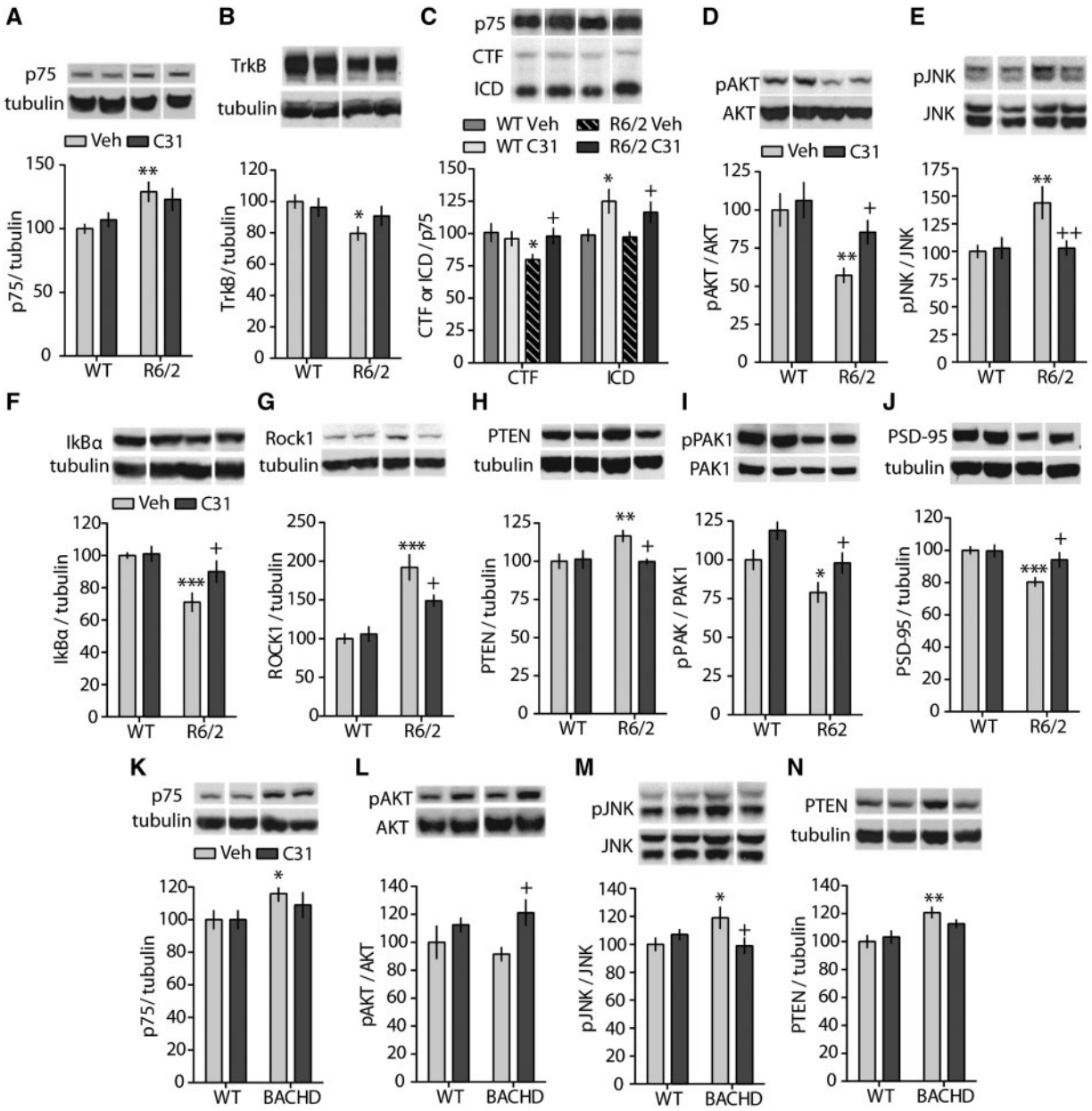

Figure 2. LM11A-31 initiates $p75^{NTR}$ cleavage and normalizes $p75^{NTR}$-associated signalling in striatum of R6/2 and/or BACHD mice. (**A–J**) Representative western blots of striatal homogenates from WT and R6/2 mice treated with vehicle (Veh) or LM11A-31 (C31) depicting: (A) full-length $p75^{NTR}$, (B) TrkB, (C) p75-CTF and -ICD, (D) pAKT, (E) pJNK, (F) Iκβα, (G) Rock1, (H) PTEN, (I) pPAK1 and (J) PSD-95. (**K–N**) Representative western blots of striatal homogenates from WT and BACHD mice showing (**K**) full-length $p75^{NTR}$, (**L**) pAKT, (**M**) pJNK and (**N**) PTEN. $^{*}P < 0.05$, $^{**}P \leq 0.01$, $^{***}P \leq 0.005$ vs. their respective WT-Veh groups; $^{+}P < 0.05$, $^{++}P \leq 0.01$ vs. transgenic (R6/2 or BACHD) Veh groups; ANOVA with Fisher's LSD *post hoc* test; $n = 8$–20 mice/group. Means (± s.e.m.) were from 4 to 6 replicated runs for each mouse sample and were normalized to the WT-Veh group run on the same gel. Immunobands from one mouse per group run on the same gel and corresponding group densitometric analyses are shown. In some instances, non-adjacent bands from the same gel were juxtaposed to facilitate comparisons. These bands were separated by spaces to indicate they were not adjacent in the original gel. Tubulin or the non-phosphorylated protein from the same stripped and re-probed gel is also shown.

Striatal MSNs are enriched in the dopamine signalling protein, 32 kDa dopamine- and cAMP-regulated phosphoprotein (DARPP-32), levels of which are markedly reduced in HD patients and mouse models (18,65–68). MSNs also express $p75^{NTR}$, which can regulate DARPP-32 expression (12,17,19). Western immunoblotting showed that LM11A-31 ameliorated the deficit in striatal DARPP-32 levels in R6/2 mice (Fig. 3F). DARPP-32 levels are not significantly reduced in BACHD mice at 10 months of age (64), however, our previous work revealed that at 8 months of age these mice have DARPP-32-containing neurites that show signs of degeneration (18). In this study, DARPP32-containing MSNs of BACHD mice (Fig. 3G–I) had significantly fewer neurites (Fig. 3J) that were shorter (Fig. 3K) and tended to occupy less area (Fig. 3L) than those in WTs. LM11A-31 treatment significantly increased the neurite number and length (Fig. 3J and K), and increased area, though this latter measure was not statistically significant (Fig. 3L).

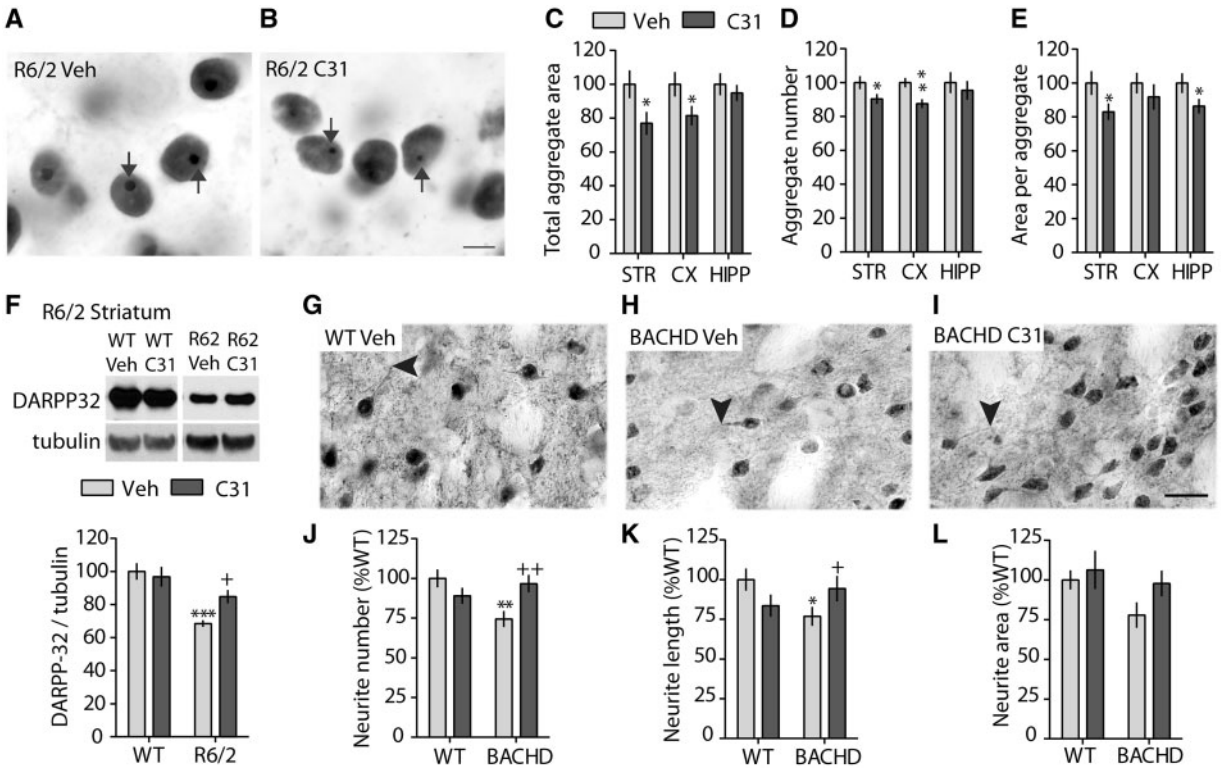

Figure 3. LM11A-31 ameliorates two principal HD neuropathologies: intranuclear Htt aggregates and striatal DARPP-32 deficits. (**A–B**) Representative photomicrographs showing nuclear Htt immunostaining in striatum (STR) of R6/2 mice treated with Veh (A) or C31 (B). Arrows indicate intranuclear Htt aggregates. Scale bar in **B**= 20 μm. (**C–E**) Quantification of the total area occupied by Htt aggregates (C), aggregate number (D) and aggregate size (E) in STR, cortex (CX), and hippocampus (HIPP) of R6/2 mice given Veh or C31 (*$P < 0.05$, **$P = 0.002$ vs. R6/2-Veh, one-tailed Student's *t*-test; $n = 11$–12 mice/group). Values in C–E are normalized to the R6/2-Veh group. (**F**) Representative Western blot for DARPP-32 showing immunobands from striatal homogenates of WT and R6/2 mice treated with Veh or C31and corresponding densitometric group analyses (***$P < 0.001$ vs. R6/2-Veh; $^{+}P \leq 0.05$; $n = 11$–12 mice/group; ANOVA with Fisher's LSD). To facilitate comparisons, non-adjacent bands from the same gel were juxtaposed and separated by spaces to indicate they were not adjacent in the original gel. Tubulin from the same stripped and re-probed gel is also shown. (**G–I**) DARPP-32 immunostaining in striata of WT-Veh mice and BACHD mice treated with Veh or C31. Scale bar in **I** = 20 μm. Arrowheads indicate distal ends of neurites. (**J–L**) Quantification of the number (**J**), length (**K**), and area (**L**) of DARPP-32-stained neurites in STR of WT and BACHD mice (*$P \leq 0.05$, **$P = 0.005$ vs. WT-Veh; $^{+}P = 0.05$, $^{++}P \leq 0.005$ vs. BACHD-Veh; $n = 7$–11 mice/group; ANOVA with Fisher's LSD). Values in (F–L) are normalized to their respective WT-Veh groups. Results are expressed as mean ± s.e.m.

LM11A-31 improves striatal cholinergic interneuron dendrite structure

Unlike MSNs, striatal interneurons are relatively preserved in HD, particularly the cholinergic sub-type (1, 69–71). While cholinergic interneurons do not decrease in number, they do undergo soma shrinkage and dendrite degeneration (72,73). These cells have been shown to contain Htt aggregates (74,75) and have disrupted electrophysiological properties, acetylcholine release and synaptic plasticity (72,76–79). Cholinergic interneurons contain low $p75^{NTR}$ levels, which increase in deleterious conditions that contribute to HD striatal degeneration, such as excitotoxicity (80,81), however, whether this increase also occurs in HD is unknown. In R6/2 mice, the area, volume and length of choline acetyltransferase (ChAT)-containing dendrites was reduced by ∼40% (Fig. 4A–D) and Sholl analysis revealed that dendritic branching was also decreased relative to WTs (Fig. 4E). LM11A-31 partially prevented all of these muHtt-associated changes in ChAT dendrites (Fig. 4).

Microglial activation is reduced by LM11A-31

The effect of LM11A-31 on striatal inflammation was as assessed using immunostaining for IBA-1, a protein expressed by activated or proliferating microglia (82–84). The striatal and hippocampal area occupied by IBA-1-stained microglia was increased in vehicle-treated R6/2 mice (Fig. 5A–E), as shown previously (18,85,86), as well as in vehicle-treated BACHD mice (Fig. 5F–J), compared to their respective WTs. LM11A-31 significantly reduced the area of IBA-1 staining in both brain areas and HD mouse models (Fig. 5D,E,I and J). The number of striatal IBA-1-positive cells did not differ between WT mice and 11 week-old R6/2 (58855 ± 3280 versus 57613 ± 7045, respectively, mean ± s.e.m, $n = 7$-8 mice/group) or 9 month-old BACHD mice (53726 ± 5750 versus 53284 ± 3152, respectively, $n = 5$-6 mice/group), similar to previous reports in which genotype differences were absent between WTs and 12 month-old BACHD and YAC128, another full-length Htt model (87,88).

Microglia undergo distinct phenotype changes when activated. At rest, their soma are oblong with ramified processes but during the activation process they appear rounded and their processes retract (89). While microglia did not proliferate in YAC128 mice, significant morphological changes occurred (87). Thus, microglial morphology was investigated in the BACHD striatum. Microglial phenotypes were diverse, however soma appeared larger, more round and less branched compared to those in WTs (Fig. 5K). Quantification revealed that microglial processes increased in number in BACHD mice while their

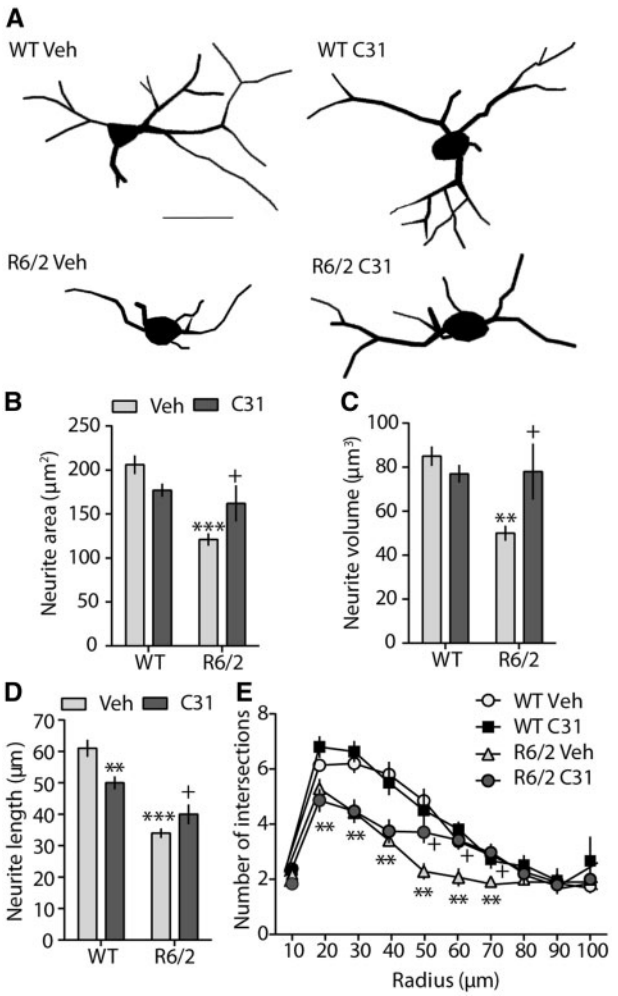

Figure 4. Dystrophic neurites of cholinergic interneurons in R6/2 striatum are mitigated by LM11A-31. (**A**) Reconstructed drawings from tracings of ChAT-immunostained interneurons in R6/2 striatum. Scale bar = 20 μm. (**B–E**) Quantification (mean ± s.e.m.) of the mean area (**B**), volume (**C**), length (**D**), and arbourizations (**E**) of ChAT-immunostained neurites in Veh- and C31-treated WT and R6/2 mice (**$P \leq 0.01$, ***$P \leq 0.001$ vs. R6/2 Veh mice; $^{+}P \leq 0.05$ vs. R6/2 Veh; $n = 9$-11/group; ANOVA with Fisher's LSD).

length and area decreased (Fig. 5L–N) but the soma area did not significantly differ from WTs (WT-vehicle: 42.1 ± 3.3 versus BACHD-vehicle: 43.1 ± 3.2 μm^2, $n = 10$ mice/group). Microglia in BACHD mice treated with LM11A-31 resembled those of WTs in process number, length and area (Fig. 5L–N).

LM11A-31 prevents dendritic spine loss in striatum and hippocampus

Dendritic spines are reduced on MSNs and CA1 pyramidal neurons of HD patients and mouse models, including R6/2 and BACHD mice (18,90–94). In the hippocampus, p75^{NTR} is localized to CA1 dendritic spines (95,96) and its post-synaptic levels are increased in HD mice (19). This increase likely contributes to the spine loss seen in HD as p75^{NTR} negatively affects spine density (97) and decreasing its levels in HD mice ameliorates spine deficits (19). LM11A-31 effects on RhoA signalling (28,29) and restoration of hippocampal LTP in an AD mouse model (24) suggests that the compound might influence spine formation. Dendritic spine density was reduced on striatal MSN dendrites in vehicle-treated R6/2 (Fig. 6A and B) and BACHD (Fig. 6C and D) mice due to a decrease in mushroom-type spines. LM11A-31 alleviated spine deficits in R6/2 mice, and, in BACHD mice and their WT littermates, increased the spine density of each morphological type examined. Spine loss also occurred on apical dendrites of hippocampal CA1 pyramidal neurons in R6/2 mice with a non-significant decrease on basal dendrites (Fig. 6E and F). Morphological analysis of apical and basal dendrites combined showed that the decrease could be attributed to fewer mushroom and thin spines (Fig. 6G). LM11A-31 significantly prevented hippocampal spine decrements in R6/2 mice (Fig. 6E–G). Density of apical and basal dendritic spines in BACHD hippocampus was not significantly affected (Fig. 6H and I). However, when apical and basal dendrites were analysed together, a significant decrease in thin and stubby spines was detected (Fig. 6J). As observed in the striatum, LM11A-31 markedly increased hippocampal spine density in both BACHD and WT mice (Fig. 6H–J).

LM11A-31 extends survival and improves motor performance in R6/2 mice

LM11A-31 administered to R6/2 mice beginning at 3.5 weeks of age until mortality did not affect the body weight of WT or R6/2 mice (Supplementary Material, Fig. S1B). Notably, a Kaplan-Meier analysis revealed that LM11A-31 significantly increased the survival of R6/2 mice (Fig. 7A). Lifespan was extended by 20 ± 6% (mean ± s.e.m; $P = 0.005$, 2-tailed Mann-Whitney test), with an increase in mean survival from 11.9 ± 0.6 to 14.3 ± 0.7 weeks.

R6/2 mice exhibit a progressive decline in general activity and exploration beginning at 4-6 weeks of age (98–101). LM11A-31 did not improve impaired motor balance and coordination of R6/2 mice on an accelerating rotarod (Fig. 7B) but significantly increased the distance moved, velocity and rearing of 7 week-old R6/2 mice in an activity chamber (Fig. 7C–E) with a tendency to decrease immobility duration ($P = 0.055$; Fig. 7F). When placed in a novel standard cage, vehicle-treated R6/2 mice perform fewer active behaviours (digging and rearing) but groom more than WTs (Fig. 7G and H). They also cross from the cage periphery to the centre less frequently (Fig. 7I) and have a higher angular velocity (speed of movement direction change) which indicates behavioural abnormalities such as stereotypies (Fig. 7J). LM11A-31 increased the number of active behaviours performed, decreased grooming, normalized periphery-to-centre transitions and decreased stereotypic behaviour in R6/2 mice (Fig. 7G–J).

LM11A-31 normalizes exploratory activity and improves cognition in R6/2 mice

Automated social phenotyping, which allows assessment of exploratory activity and unsupervised/directed learning, was performed on WT and R6/2 mice at 8-9 weeks of age for 2 weeks (Fig. 8A and B). R6/2-vehicle mice visited corners less frequently than WTs during the first 3 h in the cage suggesting reduced novelty-induced exploratory activity; LM11A-31 eliminated this deficit (Fig. 8C). Mice were required to discover and learn the new location of water bottles (corners versus cage top), with first lick latency indicating exploration and unsupervised learning. R6/2-vehicle mice took 3 times longer to discover the water location than WT-vehicle mice, while R6/2 mice given LM11A-31 located the water significantly faster than those given vehicle

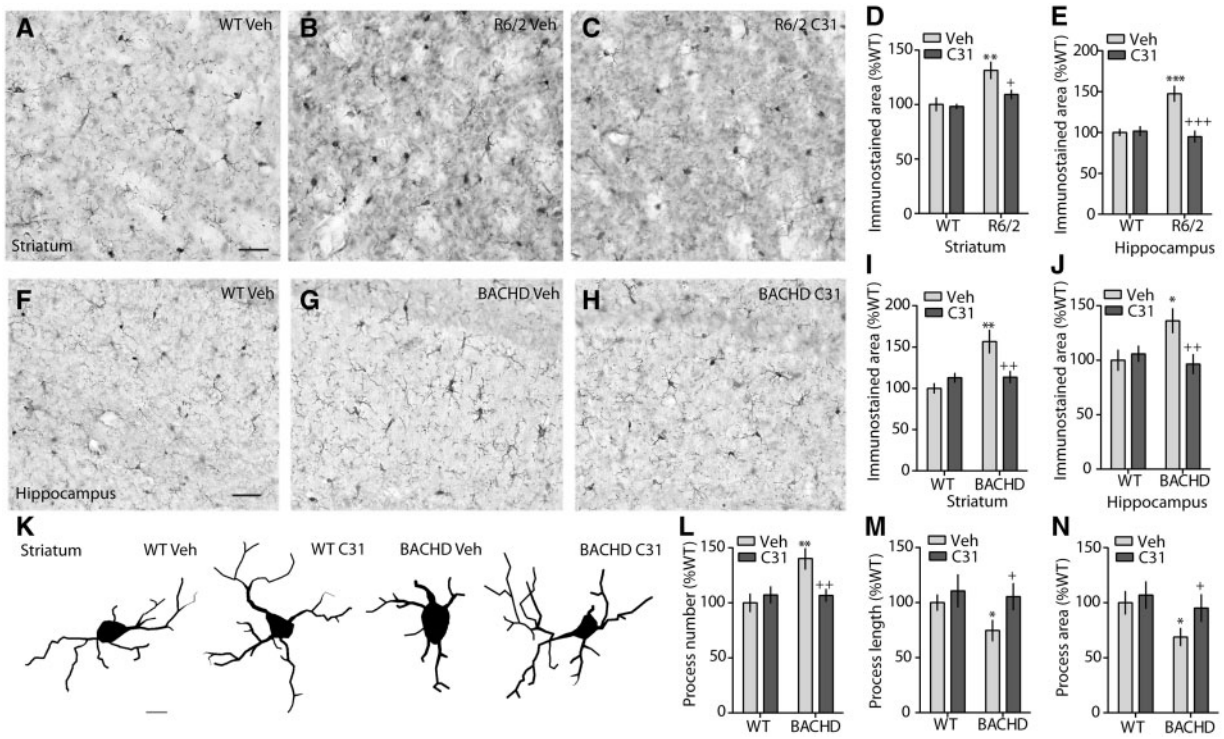

Figure 5. Inflammation is reduced by LM11A-31 in the R6/2 and BACHD striatum and hippocampus. (**A–C**) Representative photomicrographs of immunostaining for the microglial marker, IBA-1, in the striatum of a Veh-treated WT (**A**) and R6/2 mouse (**B**), and a C31-treated R6/2 mouse (**C**). Scale bar in **A** = 40 μm. (**D,E**) Quantification of the area occupied by IBA-1-immunostained soma and processes in R6/2 striatum (**D**) and hippocampus (**E**) ($^{**}P \leq 0.005$ and $^{***}P \leq 0.005$ vs. WT-Veh; $^{+}P < 0.05$ and $^{+++}P \leq 0.001$ vs. R6/2-Veh; $n = 6$-10/group; ANOVA and Fisher's LSD). (**F–H**) Representative photomicrographs of IBA-1 immunostaining in the hippocampus of a Veh-treated WT (**F**) and BACHD mouse (**G**), and a C31-treated BACHD mouse (**H**). Scale bar in **F** = 40 μm. (**I,J**) Quantification of the area occupied by IBA-1-immunostained soma and processes in the BACHD striatum (**I**) and hippocampus (**J**) ($^{*}P \leq 0.05$ and $^{**}P \leq 0.005$ vs. WT-Veh; $^{++}P < 0.005$ vs. BACHD-Veh; $n = 7$–11/group; ANOVA and Fisher's LSD). (**K**) Reconstructed drawings from tracings of microglia in the striata of WT and BACHD mice given Veh or C31. Scale bar = 6.5 μm. (**L–N**) Quantification of the mean number (L), length (M), and area (N) of IBA1-immunostained processes in striatum of WT and BACHD mice ($^{*}P \leq 0.05$ and $^{**}P \leq 0.005$ vs. WT-Veh; $^{+}P \leq 0.05$ and $^{++}P \leq 0.005$ vs. BACHD-Veh; $n = 7$–11 mice/group; ANOVA and Fisher's LSD). Results are expressed as mean ± s.e.m. and normalized to respective WT-Veh groups.

(Fig. 8D). WT mice treated with LM11A-31 also had longer lick latencies than vehicle-treated WTs however these groups performed similarly on all other measures during this testing. The above deficits in exploratory activity are most likely related to the investigation of novel stimuli and spatial information learning rather than reduced locomotion since, after the initial 3 h of exposure to the novel cage, WT and R6/2 mice visited corners with a similar frequency that decreased and then plateaued as all experimental groups became familiar with the cage (Fig. 8E). Next, corner doors were closed and the mice had to learn to nosepoke to open them and access water. R6/2-vehicle mice performed fewer nosepokes during the first 10 h and licked less for the duration of this task compared to WTs (Fig. 8F and G). R6/2 mice given LM11A-31 nosepoked and licked more frequently than those given vehicle indicating improved performance on this operant conditioning task.

During Place Learning, mice were water deprived for 16 h and were allowed access to water only after nosepoking in their least preferred corner (Fig. 8A and B). WT mice performed less nosepokes at non-reinforced corners (errors) on day 2 versus day 1 of this test, while R6/2-vehicle mice made more errors (Fig. 8H). LM11A-31-treated R6/2 mice made fewer errors on day 2, similar to WTs. Place learning was repeated after the mice were allowed free access to water and corner preference was re-established (Fig. 8A). Again, WT mice and LM11A-31-treated R6/2 mice performed fewer errors than R6/2-vehicle mice (Fig. 8I), which suggests better spatial/place learning and memory.

LM11A-31 mitigates motor, psychological and cognitive deficits in BACHD mice

Body weights of vehicle-treated BACHD mice at 2 months of age and throughout the 28 weeks of treatment were significantly greater than WT mice, as previously reported (18,63,101), and were unaffected by LM11A-31 (Supplementary Material, Fig. S2A). When mice were allowed to freely explore an activity chamber at 4 and 5 months of age, vehicle-treated BACHD mice travelled less distance and more slowly (Supplementary Material, Fig. S2B and C) than WT mice and also reared less (Supplementary Material, Fig. S2D). BACHD given LM11A-31 reared more frequently than those given vehicle at 4, but not 5, months of age; their distance travelled and velocity were unaltered. LM11A-31 improved the motor performance of BACHD mice on an accelerating rotarod at 3 months of age (after 1 month of treatment) but this effect was not evident at later ages (Fig. 9A).

Gait disturbances are pronounced and particularly debilitating for HD patients and can also occur in HD animal models including BACHD mice (99,102–105). Catwalk gait analysis showed that BACHD-vehicle mice had a longer stride length (Fig. 9B and C) and less paw contact with the floor when propelling forward during a step than WTs (Fig. 9D), and LM11A-31 normalized these measures (Fig. 9B–D). BACHD mice differ from WTs in inter-paw coordination or the temporal relationship between anchor and target paw placement during a step cycle (phase

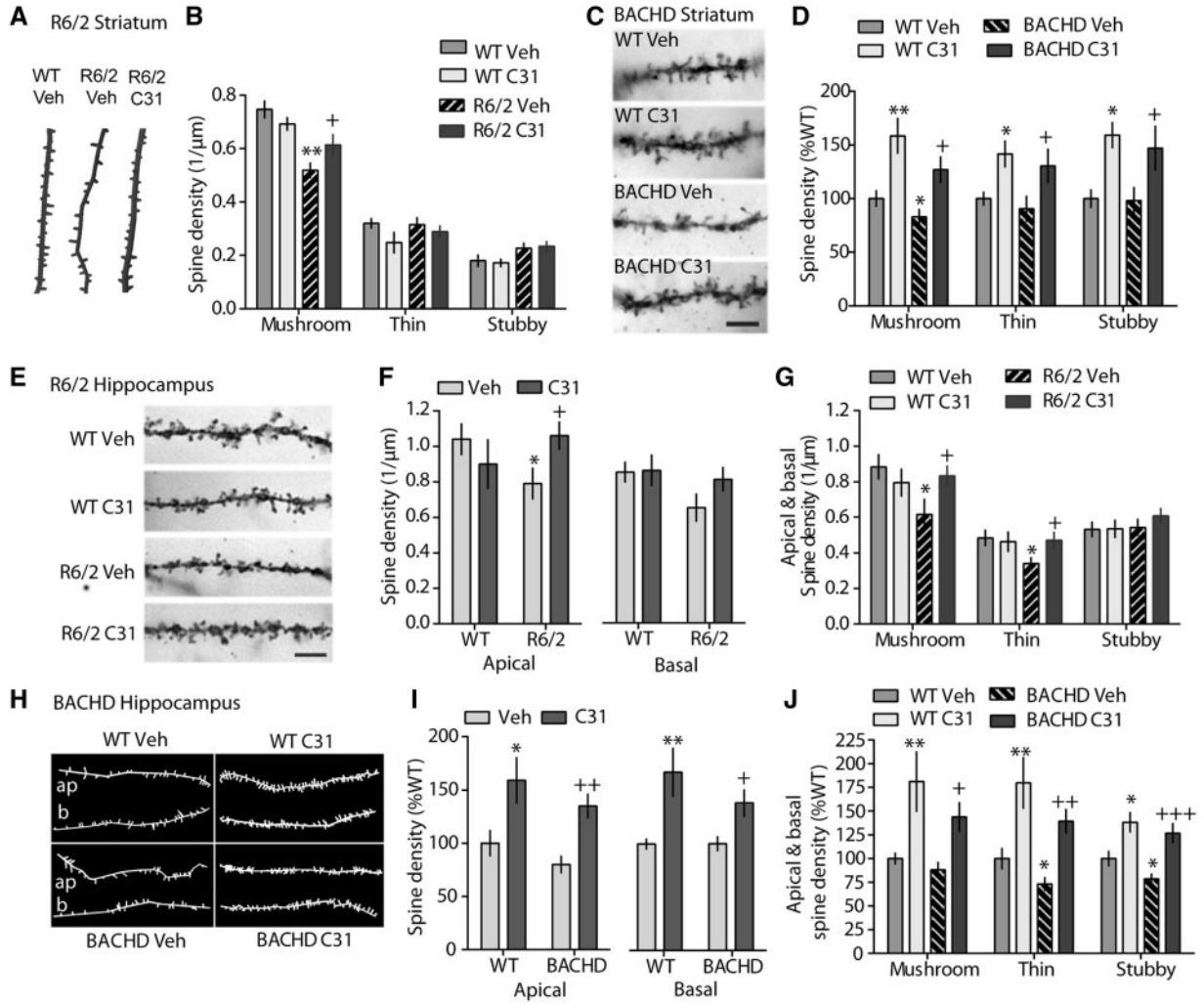

Figure 6. LM11A-31 ameliorates dendritic spine loss in striatum and hippocampus of R6/2 and BACHD mice. (**A–B**) *Dendritic spine density in R6/2 striatum:* Reconstructed tracings (A) of striatal MSN dendrite segments of WT and R6/2 mice and quantification (B) of their spine morphology (**$P \leq 0.002$ vs. WT-Veh; $^{+}P = 0.02$ vs. R6/2-Veh; $n = 6$-10 mice/group). (**C–D**) *Dendritic spine density in BACHD striatum:* Representative photomicrographs (**C**) of dendrite segments of Golgi-stained MSNs of Veh- or C31-treated WT and BACHD mice (Scale bar = 5 μm) and quantification (**D**) of their spine morphology (*$P \leq 0.05$, **$P \leq 0.005$ vs. WT-Veh; $^{+}P \leq 0.05$ vs. BACHD-Veh; $n = 7$-10 mice/group). (**E–G**) *Dendritic spine density in R6/2 hippocampus:* Representative photomicrographs (E) showing dendrite segments of golgi-stained CA1 pyramidal neurons in hippocampus of Veh- or C31-treated WT and R6/2 mice (Scale bar = 5 μm) and quantification of spine density (F) and morphology (**G**) (*$P \leq 0.05$ vs. WT-Veh; $^{+}P \leq 0.05$ vs. R6/2-Veh). (**H–J**) *Dendritic spine density in BACHD hippocampus:* Reconstructed tracings (**H**) from a segment of an apical (ap) and a basal (b) dendrite on CA1 pyramidal neurons of Veh- or C31-treated WT and BACHD mice and quantification of their spine density (I) and morphology (J) (*$P \leq 0.05$, **$P \leq 0.01$ vs. WT-Veh; $^{+}P \leq 0.05$, $^{++}P \leq 0.01$, $^{+++}P \leq 0.001$ vs. BACHD-Veh). In BACHD mice, Golgi staining was performed in two sets and results were normalized to the WT-Veh group of that staining set. All results are from $\geq 3^{rd}$ branch order dendrites, expressed as mean ± s.e.m., and statistical significance was determined by an ANOVA with Fisher's LSD.

dispersion). BACHD mice perform more diagonal, girdle, and ipsilateral phase dispersions than WTs (Fig. 9E). These coordination abnormalities were alleviated in BACHD mice treated with LM11A-31. The average intensity of paw contact with the floor did not differ between BACHD and WT mice (WT-vehicle: 36.7 ± 0.3, $n = 17$ mice, versus BACHD-vehicle: 36.9 ± 0.4 $n = 21$ mice, intensity units from 0-255), as shown previously (103), suggesting that, although the transgenics weigh more, their gait abnormalities are unlikely attributable to weight supporting limb adjustments (103). Finally, the order in which BACHD mice place their forelimbs (F) and hind limbs (H) during a step sequence significantly differed from WTs in that they used the footfall pattern *cruciate a* [right F (RF) - left F (LF) - RH - LH] more frequently and the *cruciate b* pattern [LF - RF - LH - RH] less (Fig. 9F); alternating step sequences (Aa, Ab) were not significantly affected. The footfall patterns of BACHD mice were normalized by LM11A-31 treatment.

Anxiety-like behaviours are increased in BACHD-vehicle mice as evidenced by their increased time spent in the dark compartment of a light-dark box (Fig. 9G) and less time in the open sections of an elevated zero maze (Fig. 9H), compared to WTs. LM11A-31 alleviated anxiety on both of these tests (Fig. 9G and H).

A passive avoidance task was used to evaluate the effects of LM11A-31 on associative and contextual learning and memory in BACHD mice. No genotype or drug effects on task learning were detected (Fig. 9I) but during retention testing the day after training WT mice took longer to enter the aversive zone than vehicle-treated BACHD mice suggesting that WTs learned the association between this area and the aversive stimulus to a

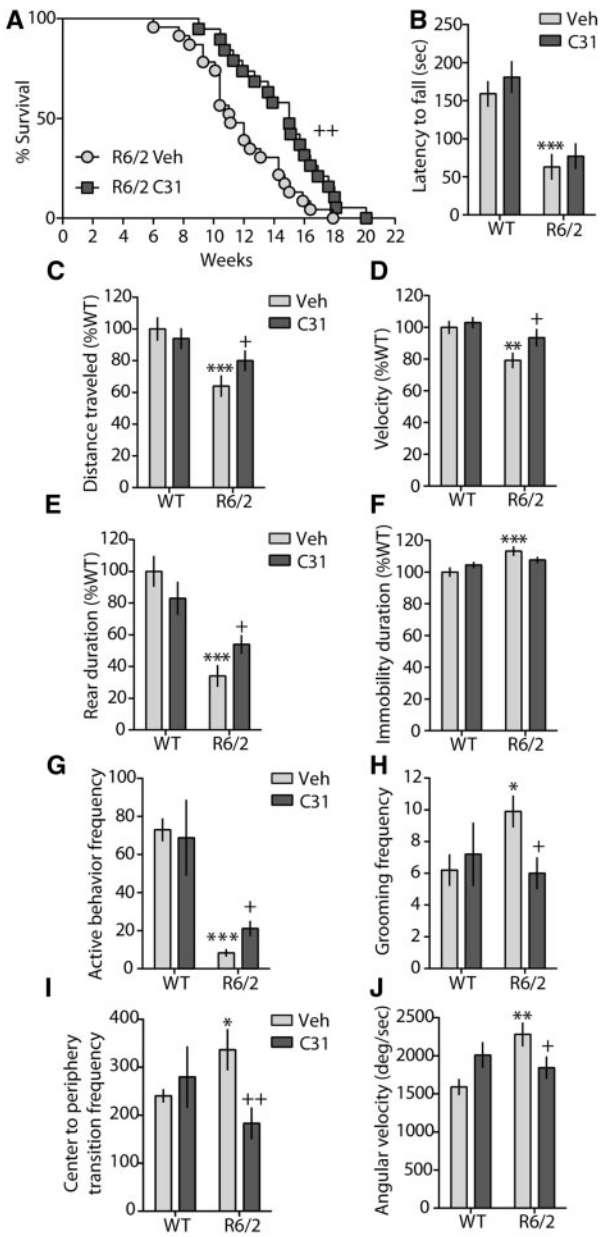

Figure 7. LM11A-31 extends survival and improves motor performance in R6/2 mice. (**A**) Kaplan-Meier analysis curve showing that C31 significantly improves survival of R6/2 mice ($^{++}P = 0.006$, log rank Mantel-Cox test; $n = 20$–24 mice/group). (**B**) Latency to fall from an accelerating rotarod was shortened in 10 week-old R6/2 mice ($^{***}P = 0.0003$ vs. WT-Veh; ANOVA and Fisher's LSD) and was not affected by C31 treatment ($n = 14$–20 mice/group). (**C–F**) During 10 min of exploring an activity chamber, deficits in travelling distance (C), velocity (D), and rearing duration (E) of R6/2-Veh mice were improved by C31 while increased immobility duration was unchanged ($^{**}P < 0.01$, $^{***}P \leq 0.001$ vs. WT-Veh; $^{+}P < 0.05$ vs. R6/2-Veh; $n = 10$-13 mice/group; ANOVA and Fisher's LSD; values normalized to WT-Veh group). (**G–J**) C31-treated R6/2 mice showed increased active behaviours (digging and rearing)(G), and decreased grooming (H), periphery-to-centre transitions (I) and angular velocity (J) compared to R6/2-Veh mice during 10 min of exploring a novel standard cage ($^{*}P \leq 0.05$, $^{**}P = 0.008$, $^{***}P < 0.0001$ vs. WT-Veh; $^{+}P \leq 0.05$, $^{++}P = 0.005$ vs. R6/2-Veh; $n = 10$–13 mice/group; ANOVA and Fisher's LSD). All results are expressed as mean ± s.e.m.

greater extent. WT mice retained this learned association 7 and 14 days after training, while vehicle-treated BACHD mice entered the aversive zone with short, pre-training latencies at 14 days (Fig. 9I). LM11A-31-treated BACHD mice exhibited significantly longer latencies to enter the aversive zone 7 and 14 days after training indicating that the compound greatly improved memory in BACHD mice.

Discussion

Recent evidence has established $p75^{NTR}$ as an important contributor to the loss of trophic support and synaptic plasticity deficits known to play a major role in HD pathogenesis (4,12,17–19). $p75^{NTR}$ is up-regulated in the HD brain, as it is under conditions of cellular stress and in other pathologies (12,16,19,106). Dysfunctional $p75^{NTR}$ signalling has been shown to negatively impact corticostriatal and hippocampal synaptic plasticity, contributing to cognitive deficits and to a lesser extent motor dysfunction in HD, and has been attributed, in part, to a $p75^{NTR}$/TrkB imbalance (4,12,15,16,19). Interestingly, a similar imbalance involving $p75^{NTR}$ and TrkA occurs in the cells that primarily degenerate in AD (107). This study showed that a $p75^{NTR}$/TrkB imbalance also exists in 11–12 week-old R6/2 and 9 month-old BACHD mice.

Although $p75^{NTR}$ functions are complex, with contributions to both pro-survival and cell death signalling (10,21,108), its potential multiplex influences on fundamental deleterious HD-associated signalling make it an enticing target for HD therapeutics. The present study supported this idea by demonstrating that the small molecule $p75^{NTR}$ ligand, LM11A-31, positively influenced many of the intracellular signalling pathways negatively affected by muHtt. Furthermore, LM11A-31 reduced Htt aggregates and alleviated striatal cholinergic interneuron degeneration in R6/2 mice. It also decreased inflammation in striatum and hippocampus and reduced dendritic spine loss in striatal MSNs and hippocampal CA1 pyramidal neurons of R6/2 and BACHD mice. Finally, it improved motor performance and cognition in both HD mouse models. Importantly, LM11A-31 increased the survival rate of R6/2 mice by 20%.

The *in vivo* engagement of $p75^{NTR}$ by LM11A-31 was supported by its induction of increased levels of the CTF and ICD cleavage products of the receptor. Proteolysis of $p75^{NTR}$ is constitutive but is also regulated by ligand binding. Sequential intra-membrane proteolysis by α- and γ-secretases generates the membrane bound CTF and then the ICD (35–38,109,110). The potential biological significance of $p75^{NTR}$ cleavage products is complex, as they have been shown to influence $p75^{NTR}$ signalling via both cell survival pathways (*e.g.* $p75^{NTR}$'s potentiation of Trk signalling by increasing activated AKT) and death pathways, depending on the cell type and context, as well as neurite outgrowth (36–38,110). However, the roles of the CTF and ICD in the HD brain are unknown. Of interest, CTF levels were significantly decreased in R6/2 mice which could be caused by reduced extracellular ligand-induced proteolysis of $p75^{NTR}$ due to decreased BDNF levels and/or less constitutive cleavage (4,37,110). The current findings, along with prior *in vitro* and *in vivo* studies suggesting direct LM11A-31/$p75^{NTR}$ interactions (23,31,33), indicate that proteolysis is likely triggered directly by compound-receptor interactions, though the possibility of indirect mechanisms remains for further investigation.

LM11A-31 was shown previously to prevent degenerative signalling while triggering trophic signalling in numerous neurodegenerative conditions (21,22). In the present study, similar LM11A-31 effects on $p75^{NTR}$ signalling were observed in the presence of muHtt. LM11A-31 partially to completely normalized JNK, RhoA, NFκB and AKT signalling in the striatum of R6/2 and/or BACHD mice, which could underlie its mitigation of diverse and fundamental HD pathologies (see Fig. 1), including:

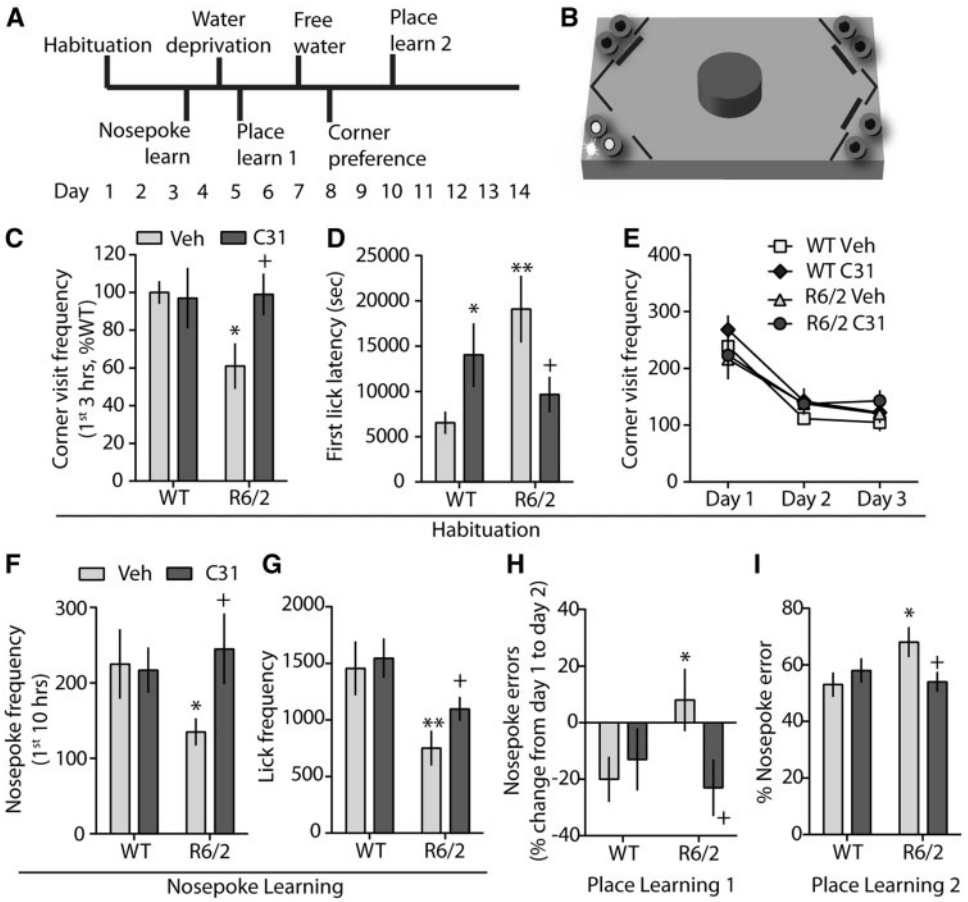

Figure 8. LM11A-31 improves exploratory activity and learning of R6/2 mice in a novel social environment. (**A**) *Testing timeline*: during the 2 weeks WT and R6/2 mice were group-housed in an IntelliCage ($n = 10$–13 mice/group). (**B**) *IntelliCage schematic*: during place learning, all doors are closed (thick lines) and water is only accessible from each mouse's least preferred corner after opening the door (no thick line) with a nosepoke (bottom left, LED light illuminated). (**C–E**) *Habituation*: water is available from all corners without nosepoke. R6/2-Veh mice visited corners less frequently during the first 3 h in the cage (C) and had longer first lick latencies (D); C31 corrected these deficits. Deficits were not due to decreased locomotion as all groups visited corners with equal frequencies after the first 3 h (E). (**F–G**) *Nosepoke learning*: doors were closed preventing water access unless opened with a nosepoke. R6/2-Veh mice performed fewer nosepokes for first 10 h (F) and licked less (G) over 24 h; C31 normalized these behaviours. (**H–I**) *Place learning*: During place learning I (H), R6/2-Veh mice performed more errors on the second versus first day while WTs and C31-treated R6/2 mice made fewer nosepoke errors. Similarly during 4 days of place learning II (I), WTs and C31-treated R6/2 mice performed fewer combined errors than R6/2-Veh mice. $^{*}P < 0.05$, $^{**}P < 0.01$ vs. WT-Veh; $^{+}P < 0.05$ vs. R6/2-Veh, ANOVA and Fisher's LSD. Results are expressed as mean ± s.e.m.

Htt aggregation, which may be affected by AKT (111–113) and RhoA/ROCK1 signalling (114–116); DARPP-32 and cholinergic interneuron morphological abnormalities, which may involve JNK (117), RhoA (118,119) and AKT (40,66) pathways; and inflammatory reactions, responsive to NFκB signalling (44–46).

The precise mechanism by which LM11A-31 modulates $p75^{NTR}$ to increase survival and decrease degenerative signalling remains unknown. Though nerve growth factor (NGF) has been shown to provide neuroprotection and improve cognition in an HD mouse model (120), and LM11A-31 has structural and chemical features similar to the NGF loop 1 β-turn domain which interacts with $p75^{NTR}$ (22,23), the compound's activities are distinct from those of NGF. Most notably, previous *in vitro* studies showed that unlike the NTs, LM11A-31 does not activate the NGF receptor TrkA, or other Trks (23). However, like NGF, in some conditions LM11A-31 recruits signalling adaptors to $p75^{NTR}$ to promote $p75^{NTR}$-dependent activation of downstream pathways and cell survival. These protective effects are also observed in 3T3 cells that lack Trks. In addition, though the $p75^{NTR}$ ligand proNGF promotes cell death via $p75^{NTR}$ in susceptible cells, LM11A-31 does not have this effect, and in fact antagonizes proNGF-induced apoptotic cell death (23). Furthermore, in a model of neuronal Aβ toxicity, LM11A-31 was protective where NGF was not, and added NGF antagonized the protective effects of the compound (24). Together, these results suggest that LM11A-31 has system/state-dependent effects which may involve agonism of $p75^{NTR}$-coupled survival signalling and/or antagonism of degenerative signalling. Finally, no activation of TrkB was observed in neurons treated with LM11A-31, suggesting the compound did not promote BDNF secretion (23). Thus, it seems unlikely that the beneficial effects of LM11A-31 seen in this study involve potentiation of NT levels or actions, though this possibility cannot as yet be completely ruled out.

LM11A-31 reduced the size and/or number of intranuclear Htt aggregates in the striatum, cortex and hippocampus suggesting that the ligand mitigates production and/or accumulation of muHtt oligomers. These results could be due to LM11A-31 activation of AKT or reduction in RhoA/ROCK signalling. AKT activation has been reported to decrease muHtt aggregation and toxicity directly by phosphorylating Htt or indirectly

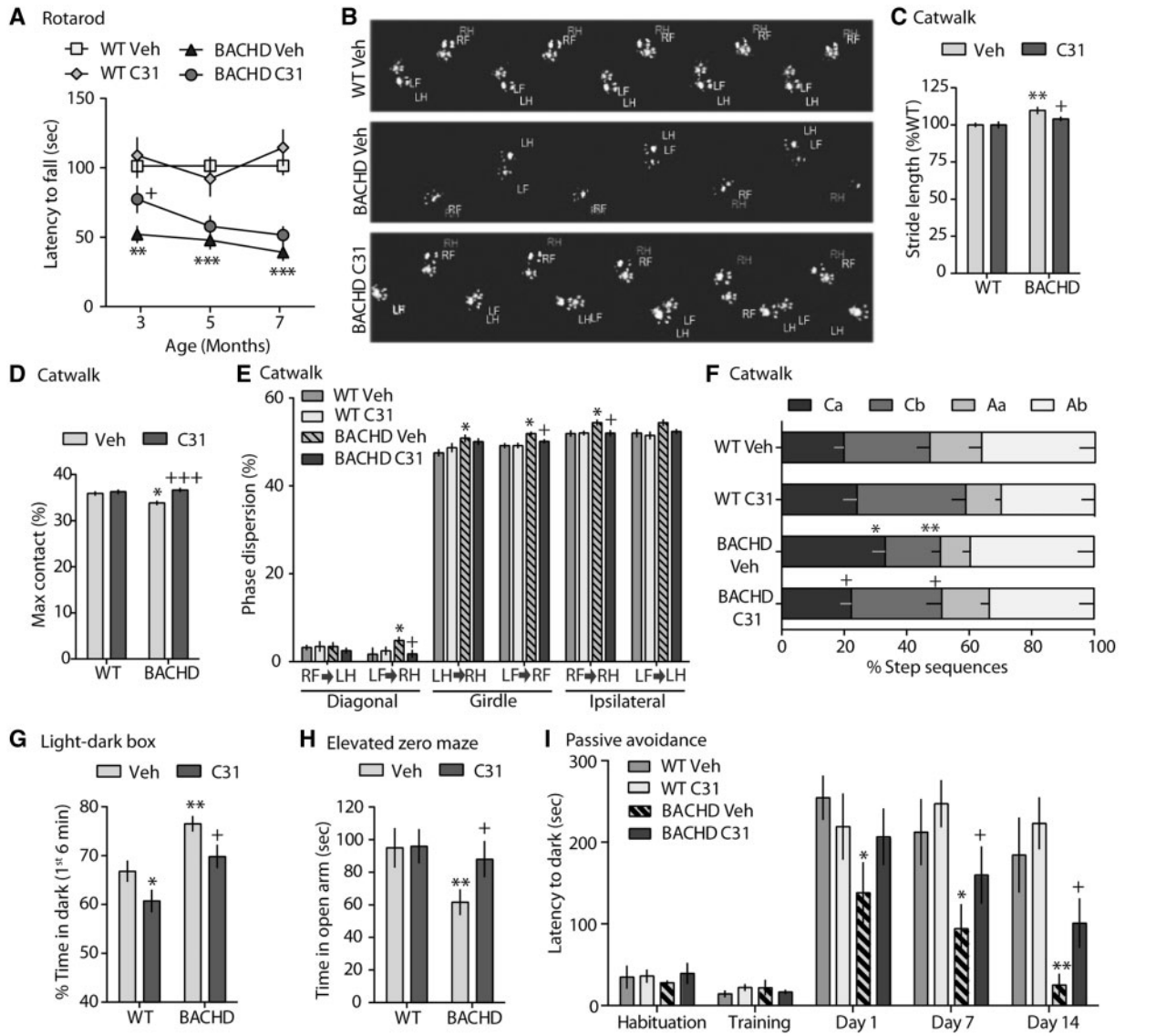

Figure 9. Motor performance and memory are improved by LM11A-31 while anxiety is palliated in BACHD mice. (**A**) Performance of BACHD mice at 3, 5 and 7 months of age on an accelerating rotarod. (**B–F**) Gait abnormalities were assessed using Catwalk footprint visualizations (**B**) showing the inter-paw distance and footfall patterns of right (R) and left (L) forelimbs (F) and hind limbs (H). Gait measures analysed included: (C) stride length, (D) maximum (Max) contact (i.e. time paws maximally contact floor), (E) phase dispersion (*i.e.* time of initial target paw contact expressed as a percentage of the step cycle time of an anchor paw; anchor-target paw placements are diagonal, girdle, and ipsilateral), and (F) step sequences [i.e. percent of times mice perform pre-defined footfall patterns: cruciate a or b [*Ca*: right front paw (RF) - left front paw (LF) - right hind paw (RH) - left hind paw (LH); *Cb*: LF - RF - LH - RH] and alternate a or b [*Aa*: RF - RH - LF - LH; *Ab*: LF - RH - RF - LH]. (**G–H**) Anxiety-like behaviour was assessed using a light-dark box (G) and an elevated zero maze (H). (I) A passive avoidance task was used to evaluate memory in WT and BACHD mice, with retention testing one day after aversive learning and extinction tests on Days 7 and 14. Statistical significance was determined with an ANOVA and a Fisher's LSD, except for phase dispersion analysis, which used a 2-way ANOVA with Tukey's multiple comparisons *post hoc* test. $^{*}P \leq 0.05$, $^{**}P \leq 0.01$, $^{***}P \leq 0.001$ vs. WT Veh; $^{+}P \leq 0.05$, $^{+++}P \leq 0.001$ vs. BACHD Veh; $n = 20$–22 mice/group, except passive avoidance $n = 10$/group.

by promoting proteasomal degradation of Htt via increasing arfaptin2 activity (40,111,112). Inhibiting the ROCK pathway enhances muHtt degradation and aggregation while improving motor function in R6/2 mice (52,53,114–116). The aggregate load reduction has also been associated with improved cognition and/or motor performance in HD mice (5,18,121–125). Thus, LM11A-31's effects on muHtt metabolism may contribute to its restorative effects on motor performance and cognition.

LM11A-31 also prevented spine morphology abnormalities and loss in R6/2 and BACHD mice and, in the latter model, elevated spine density to levels greater than that observed in vehicle-treated WT mice. Post-synaptic $p75^{NTR}$ levels are elevated in hippocampus of HD mice (19) which likely contributes to spine loss as $p75^{NTR}$ negatively affects spine density (97) and decreasing levels of the receptor in HD mice mitigates spine deficits (19). While LM11A-31 does not affect $p75^{NTR}$ levels, it activates AKT and PAK signalling, which can positively regulate spine formation, morphology and/or function (126–129), while decreasing RhoA-associated signalling which can negatively affect spines (119,130). LM11A-31 also prevented the decline in striatal PSD-95 levels in R6/2 mice. Taken together, these results suggest that LM11A-31 can reduce $p75^{NTR}$-associated synaptic dysfunction seen in HD (19). The positive effects of LM11A-31 on synaptic-related signalling /proteins and spine density provide

substrate mechanisms for its beneficial effect on cognition in R6/2 and BACHD mice.

While LM11A-31 largely normalized $p75^{NTR}$ signalling in the striatum, it only partially recovered motor behaviour. It mildly improved locomotion and exploratory activity but did not affect the rotarod performance of R6/2 mice, and, in BACHD mice, general locomotor activity and motor learning/balance were ameliorated by LM11A-31 in early but not later stages of treatment. Incomplete motor recovery is consistent with the partial reversal of DARPP-32 deficits shown in this study, and the lack of significant improvement in rotarod performance and corticostriatal synaptic plasticity seen in the Hdh^{Q111} knock-in HD mouse model when $p75^{NTR}$ expression is decreased (19). Thus, other signalling pathways and extra-striatal brain areas involved in motor function are likely not affected by LM11A-31, at least with the dosing protocol used in this study. Future investigations will examine whether other LM11A-31 dosing paradigms will be more effective against motor deficits and neurodegeneration.

LM11A-31 reduced the stereotypic behaviours displayed by R6/2 mice. Behavioural inflexibility and stereotypies, including cognitive impairments related to attentional set shifting or choreiform movements in HD patients, are associated with striatal dopamine imbalance and disrupted corticostriatal communication and thalamostriatal inputs to cholinergic interneurons (131–135). Thus, the reduction in repetitive behaviours, including grooming, seen with LM11A-31 treatment may arise from the compound's partial restorative effects on DARPP-32 levels and prevention of cholinergic interneuron degeneration.

Second only to chorea, gait abnormalities are the most prominent motor dysfunction exhibited by HD patients and can be distinguished in pre-symptomatic gene mutation carriers (105,136–138). Recuperative effects of LM11A-31 were seen on aspects of impaired gait in BACHD mice at 9 months of age, including stride length, step sequence and brake/propulsion transitions. These results suggest that, despite the relatively small effects of LM11A-31 on locomotion, the compound does alleviate gait disturbances, a major quality of life factor for HD patients because of loss of independence and fall risk (137–139), which could be easily and reliably used as a clinical trial outcome measure (136).

In conclusion, these studies demonstrate that LM11A-31, when administered once per day for 5-6 days per week, significantly reduced motor, cognitive, psychiatric and neuropathological abnormalities in two HD mouse models. Taken together, these results provide validation that a small molecule ligand modulating $p75^{NTR}$, a receptor critically positioned in survival and neurodegenerative signalling, may serve as an effective HD therapeutic. LM11A-31 has successfully completed Phase I safety and pharmacokinetic clinical studies in normal subjects and is therefore a viable lead candidate for HD clinical testing.

Materials and Methods

Study design

This study aimed to establish $p75^{NTR}$ as a feasible therapeutic target for HD by determining the effectiveness of a small molecule $p75^{NTR}$ ligand, LM11A-31, on multiple HD-related signalling, neuropathological and behavioural endpoints in both male R6/2 and BACHD mice. R6/2 mice are particularly beneficial for testing therapeutics because they develop HD symptoms rapidly and reliably; BACHD mice better represent the genetic component of HD and have a slower disease progression which allows targeting of early degenerative mechanisms (101). These experiments used a 2 × 2 study design [WT/transgenic X vehicle/LM11A-31] with the random group assignment. Group size needed to obtain statistical significance was determined based on previously published studies using these mice (18,101,140). LM11A-31 was dissolved in sterile water and given to experimental groups after 4 h of fasting at 50 mg/kg (10 ml/kg) via oral gavage once daily 5–6 days/week. Vehicle control groups received water in the same manner. This dose was used based on brain concentrations (23,32) and biological effects determined in previous *in vitro* and *in vivo* studies (23,24,26,32,34). Mouse brain half-life of LM11A-31 following a single oral-gavage dose of 50 mg/kg is 3-4 h (32). R6/2 mice and their WT littermates were treated in multiple cohorts with dosing started at 4 weeks of age. Cohort 1 of R6/2 mice was dosed throughout their lifespan to determine the effects of LM11A-31 on survivability ($n = 20$-24/group). Cohorts 2 and 3 were dosed for ~7 weeks. Cohort 2 mice received rotarod testing and one brain hemisphere was used for immunohistochemistry and the other for Western immunoblotting ($n = 18$-22/group). Cohort 3 mice were tested in an activity chamber, then the IntelliCage, followed by the novel home cage and brains were used for Golgi staining ($n = 10$-13/group). BACHD mice were treated from 2 to 9 months of age in 2 cohorts (total $n = 20$-22/group) that received all behaviour tests. Cohort 1 brains were used for modified Golgi staining and, for Cohort 2, one brain hemisphere was used for immunostaining and the other for Western immunoblotting. All dosing, behaviour testing, and histological and quantitative analyses were conducted by experimenters that were blind to the treatment and genotype conditions.

$p75^{NTR}$ ligand

LM11A-31 [2-amino-3-methyl-pentanoic acid (2-morpholin-4-yl-ethyl)-amide] is a water soluble isoleucine derivative identified via *in silico* screening for compounds corresponding to the NGF loop 1 β-turn domain that interacts with $p75^{NTR}$ (22,23). Its chemical structure, pharmacokinetics and pharmacodynamics have been detailed previously in published reports from our laboratories (23,24,26,32). LM11A-31 successfully completed Phase 1 clinical trials evaluating safety and pharmacokinetics in healthy individuals (Longo et al., 2015, personal communication). LM11A-31 in a sulphate salt form [(2*S*,3*S*)-2-amino-3-methyl-N-(2-morpholinoethyl) pentanamide] was used in this study and was custom manufactured by Ricerca Biosciences at >99% purity. The MW of this salt is 439.34 versus the free base MW of 243.35 (50 mg of the salt contains 30 mg of the free base).

Mice and genotyping

All animal procedures were conducted in accordance with the National Institutes of Health Guide for the Care and Use of Laboratory Animals using protocols approved by the Institutional Animal Care and Use Committee at Stanford University. These protocols included efforts to minimize animal suffering and numbers used. Mice were group-housed (3–5 mice/cage), except aggressors if fighting occurred, and received cotton nestlets, paper tubes and rodent chow *ad libitum*. Tail DNA was used for genotyping via real-time PCR and CAG repeat number measurement via ABI GeneMapper 4.0 by Laragen Inc. For R6/2 mice, breeding pairs were purchased from Jackson Laboratories [female hemizygous ovarian transplant

B6CBA-TgN (HD exon1)62; JAX stock #006494]. These mice are transgenic for the 5′ end of the human HD gene carrying 100-150 glutamine (CAG) repeats (68). This study used male R6/2 mice that had an average of 125 ± 2.6 (mean ± SD) CAG repeats. Male BACHD mice, and their WT littermates, were also purchased from Jackson (stock #008197) and are a bacterial artificial chromosome mediated transgenic model that expresses full-length human muHtt with 97-98 CAG repeats (63). BACHD mice used in this study all had 98 CAG repeats.

Behaviour testing

Behaviour tests were chosen for each mouse model based on the severity of HD phenotypes and/or the existence of published reports for the test in that model. To evaluate the effects of LM11A-31, behaviour tests that had previously shown significant genotype differences were used (101,103,141,142). Because R6/2 mice have severe symptoms, are prone to stress-induced seizures, and have a short lifespan, the number of behaviour tests that can be performed in a cohort is limited compared to the BACHD mice. R6/2 mice received the following behaviour tests at the ages denoted during the light phase of the light/dark cycle: activity chamber (7 weeks), accelerating rotarod (10 weeks), Intellicage (8–10 weeks), and novel home cage (10 weeks). BACHD mice received the following behaviour tests at the ages denoted during the dark phase of the light/dark cycle: accelerating rotarod (3, 5 and 7 months), activity chamber (4 and 5 months), light-dark box (4 and 5 months), elevated zero maze (7 months), Catwalk (9 months), and passive avoidance (9 months); tested were separated by at least a week.

Behaviour testing procedures will be described briefly here and in more detail in the Supplementary Materials. Both R6/2 and BACHD mice underwent accelerating rotarod (4 to 40 rpm over 5 min) and activity chamber testing, as described previously (18). IntelliCage (New Behaviour AG) testing involved automated recording of home cage behaviours and exploratory activity of mice living in social groups ($n = 13$–16 mice/cage). R6/2 mice and their WT littermates ($n = 10$-13/group) were moved to Intellicages for 2 weeks starting at 8 weeks of age. They were implanted subcutaneously with RFID-transponders under isoflurane anaesthesia for individual tracking. Testing paradigms used were similar to those used previously in R6/2 mice (141,142). Mice explored the cage for 3 days with all 4 corner doors open and water available from each corner. Corner doors were shut for the next 2 days and the mice must learn to nosepoke in the door vicinity to open them and receive water (Nosepoke Learning); the preferred drinking corner for each mouse was determined. After 16 h of water deprivation, all corner doors were closed for 2 days and mice only received water via a nosepoke at their least preferred corner (Place Learning 1); correct nosepokes were paired with LED light illumination. This learning process was repeated and mice were again only permitted to drink from their least preferred corner (Place Learning 2). One week after mice were removed from the IntelliCage, a subset was allowed to explore a novel standard home cage for 10 min. Their behaviour was recorded by an overhead camera and then analysed with Ethovision XT software v8.5 (Noldus). Gait abnormalities were assessed in BACHD mice, similar to that shown previously (103), using the video-based CatWalk XT system (v9.1, Noldus). After training mice to traverse the walkway, test sessions of three consecutive runs were conducted and averaged. Anxiety-like behaviour was evaluated in BACHD mice using a light-dark box and an elevated zero maze. In the light-dark box, mice were allowed 15 min of exploration in a chamber with two compartments; one dimly lit (10 lux), the other brightly lit (800 lux). Total time spent in each compartment was digitally recorded and analysed using tracking software (Med Associates Inc.). For the elevated zero maze, BACHD mice were allowed 5 min of exploration of a circular walkway that had two portions enclosed with walls and two equal portions without walls; time spent in each section of the maze was analysed. The passive avoidance test was conducted in a two compartment chamber (Gemini^{TM} Avoidance System, SD Instruments): one light and one dark. Tactile cues were added to the floor of the light compartment. Mice were allowed to explore the apparatus and, when they entered the dark chamber, received a mild foot shock. Testing for retention of the pairing of the aversive stimulus with the preferred compartment occurred 1 day later and was expressed as latency to enter the dark chamber. Extinction of the learned association was assessed 7 and 14 days later.

Western immunoblotting

One hour post-injection with LM11A-31 or vehicle, R6/2 and BACHD mice along with their respective WT littermates ($n = 8$–20 mice/group) were deeply anaesthetized with avertin and their brains were removed rapidly. Striatum was dissected from the brains and flash frozen at -80 °C. Brain tissue was prepared for Western blotting, as described previously (18). Briefly, tissue homogenates were prepared in RIPA lysis buffer containing protease and phosphatase inhibitors. Protein samples from each genotype and treatment group were electrophoresed through a 26 well NuPAGE 4–12% Bis-Tris Gel with MOPS SDS running buffer (Invitrogen) and transferred to polyvinylidene difluoride membranes. Membranes were probed using the following antibodies: p75^{NTR} (Promega); TrkB (Millpore); phospho(p)-AKT (Ser473) and AKT (Cell Signaling); pJNK (Thr183/Tyr185) and JNK (Cell Signaling); IκB-α (Santa Cruz Biotechnology); ROCK1 (Cell Signaling); PTEN (Cell Signaling); pPAK1 (Thr423)/PAK2 (Thr402; Cell Signaling) and PAK1 (Abcam); PSD-95 (Millpore); and DARPP-32 (Epitomics). All blots were also stripped and reprobed with α-tubulin monoclonal antibody (Sigma) as a loading control. Immunoreactive bands were manually outlined and densities were measured using Un-Scan-It gel software (v6.1, Silk Scientific). The densities of phosphoprotein-immunoreactive bands were expressed as a fraction of the band for the total protein and all other bands were expressed as a fraction of tubulin in the same lane after reprobing. Samples were run 4 to 6 separate times per mouse and data was normalized to the WT-vehicle group of that gel then averaged. In the Western blot figures, some non-adjacent bands were moved together for comparison purposes; these were separated by spaces.

Immunohistochemistry procedures and quantification

Mice were deeply anaesthetized with avertin and transcardially perfused with saline solution. One brain hemisphere was used for Golgi staining and the other was immersion-fixed overnight in 4% paraformaldehyde in 0.1M phosphate buffer (PB; pH 7.4), cryoprotected in 30% sucrose/PB, and sectioned (40 μm, coronal) using a freezing microtome. Free-floating sections were processed for immunocytochemical localization of Htt (1:200; clone EM48, Millipore), ChAT (1:800; Millpore), DARPP-32 (1:1,000; Millpore), or IBA-1 (1:1,000;

WAKO) using procedures described previously (18). Immunostaining in striatum was examined at rostral to mid-caudal levels [+1.18 to +0.02 mm relative to Bregma;(143)] with sampling fields placed ventral to and abutting the corpus callosum. For the analysis of nuclear Htt staining, the primary motor cortex (+0.98 to +0.86 mm relative to Bregma) and dorsal hippocampus (−1.7 to −2.3 mm) were also examined (143). In this latter region of the hippocampus, IBA-1 immunostaining was also quantified. Images were acquired with a Zeiss AxioImager M2 microscope, AxioCam Hrc camera and Axiovision (Zeiss) or Microlucida (MBF Biosciences) software. If immunostaining was performed in multiple sets, quantifications were normalized to the WT-vehicle group of that staining set and cohort. Intranuclear Htt accumulation was evaluated by manually tracing immunoreactive nuclei and intranuclear aggregates in the striatum (sample field 250 × 250 μm), cortex [sample field (250 × 250 μm) in cortical layers 4/5], and hippocampus [sample field (125 × 25 μm) in CA1 pyramidal layer] in one section per mouse while viewing with a 100X objective using Neurolucida v11.07 (MBF) image analysis software. Striatal volume was estimated in every 8th coronal section (40 μm) between 1.34 and −0.22 mm relative to Bregma ($n = 9$–11 mice/group) using the Cavalieri method within StereoInvestigator v11.07 (MBF). IBA-1 immunostaining was used to assess activated microglia and was analysed in 2–3 striatal and hippocampal sections per mouse [8–12 sample fields per brain area] were imaged at 20X and analysed with Image J (v1.49p) subtract background and auto-threshold commands. Microglia morphology of BACHD mice was also evaluated in the striatal fields described above by manually tracing microglia (4–5 per mouse) and their processes using Neurolucida while viewing with a 40X objective and focusing through the Z-plane. Degenerating neurites of MSNs in BACHD mice were assessed by manually tracing DARPP-32-immunostained neurons in a sample field (nine 250 × 250 μm boxes) in one section of the striatum. Neurons and neurites originating from them, were manually traced while using Neurolucida's automated scanning procedure which allows unbiased non-overlapping fields to be selected. All neurons [216 ± 10 MSNs per mouse (mean ± s.e.m.)] in every 3rd meander scan field were traced using a 40X objective while focusing through the Z-plane. Degenerating neurites of cholinergic interneurons in R6/2 mice were assessed by manually tracing ChAT-immunostained neurons, as described above for DARPP-32 neurites in BACHD mice. Except the sample field was sixteen 250 × 250 μm boxes and all neurons [29 ± 1.2 MSNs per mouse (mean ± s.e.m.)] in every other meander scan field were traced. Sholl analysis (Neurolucida) was performed on 10 interneuron tracings per mouse picked using a random number generator.

Stereology

Unbiased stereology was performed using the optical fractionator method to obtain counts of IBA-1 positive cells in the R6/2 striatum by an observer blind to experimental groups using StereoInvestigator software (MicroBrightField, Inc, Williston, VT) and a Zeiss AxioImager M2 microscope. The striatum was outlined using a 5X objective and every 8th section was analysed (totaling 6 to 8 sections per animal from ∼1.34 and −0.22 mm relative to Bregma). Before counting, section thickness was measured and guard zones and dissector height was determined and set. Cells were counted in a 100 μm × 100 μm counting frame inside a 200 μm × 200 μm grid using a 40X oil objective. Gunderson $m = 1$ coefficient of error for cell counts was ≤0.05.

Modified Golgi staining

Brains were immersed in modified Golgi-Cox staining solution (purchased from Drs. Deqiang Jing and Francis Lee at Cornell University) and processed as described previously (18). Dendritic spine density was determined by manually tracing Golgi-stained MSNs in the dorsal striatum and CA1 pyramidal cells in the dorsal hippocampus while viewing and adjusting focus at 100X using Neurolucida. Neurons (3–5/mouse) that minimally overlapped adjacent neurons were selected. For the striatum, all branches from one dendritic tree were traced per neuron and for the hippocampus, 3 basal and 3 apical dendrite segments (≥100 μm) were traced. Dendritic branch orders 3 and higher were analysed, as these are the most affected in HD mice (93,144). Spine morphology, including mushroom, thin and stubby, was also recorded using criteria defined elsewhere (145).

Statistical Analysis

Statistical significance was determined via a one-way analysis of variance (ANOVA) with a Fisher's LSD *post hoc* test and/or a Student's *t*-test for paired comparisons or Mann-Whitney for non-parametric tests using GraphPad Prism v6. A repeated measures (RM) ANOVA was used for body weight. Values that were two standard deviations from the mean (criteria determined *a priori*) were removed as statistical outliers. Results are expressed as group mean ± standard error of the mean (s.e.m.) and statistical significance was set at $P \leq 0.05$.

Supplementary Material

Supplementary Material is available at HMG online

Acknowledgements

The research was designed by D.A.S and F.M.L.; D.A.S, N.P.B, E.F., S.S., M.M., S.A., C.M.H. and C.C. performed the research; M.S. provided resources; D.A.S., N.P.B., E.F. and S.S. analysed data; D.A.S. wrote the manuscript; and S.M.M. and F.M.L. critically revised it. The modified Golgi staining kit was purchased from Drs. Francis Lee and Deqiang Jing under a material transfer agreement between Cornell University and Stanford University.

Conflict of Interest statement. F.M.L. and S.M.M. are listed as inventors on patents relating to LM11A-31 which are assigned to the University of North Carolina, University of California (UC), San Francisco and the Dept. of Veterans Affairs (VA). F.M.L. and S.M.M. are entitled to royalties distributed by UC and the VA per their standard agreements. F.M.L. is a principal of, and has a financial interest in PharmatrophiX, a company focused on the development of small molecule ligands for neurotrophin receptors which has licensed several of these patents.

Funding

This work was supported by the National Institutes of Health [R21 NS081089-01 to F.M.L., P30 NS069375-05 to M.S.]; Taube Philanthropies to F.M.L; Koret Foundation [12-0160 to F.M.L.], Jean Perkins Foundation to F.M.L., and the Veterans Administration to S.M.M. Funding to pay the Open Access

publication charges for this article was provided by the National Institutes of Health [R21 NS081089-01], Taube Philanthropies, and Koret Foundation [12-0160].

References

1. Vonsattel, J., Myers, R., Stevens, T., Ferrante, R., Bird, E. and Richardson, E.J. (1985) Neuropathological classification of Huntington's disease. *J. Neuropathol. Exp. Neurol.*, **44**, 559–577.
2. Walker, F.O. (2007) Huntington's disease. *Lancet*, **369**, 218–228.
3. Group, HsDCR. (1993) A novel gene containing a trinucleotide repeat that is expanded and unstable on Huntington's disease chromosomes. *Cell*, **72**, 971–983.
4. Zuccato, C. and Cattaneo, E. (2007) Role of brain-derived neurotrophic factor in Huntington's disease. *Prog. Neurobiol.*, **81**, 294–330.
5. Gharami, K., Xie, Y., An, J.J., Tonegawa, S. and Xu, B. (2008) Brain-derived neurotrophic factor over-expression in the forebrain ameliorates Huntington's disease phenotypes in mice. *J. Neurochem.*, **105**, 369–379.
6. Reichardt, L.F. (2006) Neurotrophin-regulated signalling pathways. *Philos. Trans. R. Soc. Lond. B. Biol. Sci.*, **361**, 1545–1564.
7. Roux, P.P. and Barker, P.A. (2002) Neurotrophin signaling through the p75 neurotrophin receptor. *Prog. Neurobiol.*, **67**, 203–233.
8. Coulson, E.J., Reid, K., Murray, S.S., Cheema, S.S. and Bartlett, P.F. (2000) Role of neurotrophin receptor p75NTR in mediating neuronal cell death following injury. *Clin. Exp. Pharmacol. Physiol.*, **27**, 537–541.
9. Gentry, J.J., Barker, P.A. and Carter, B.D. (2004) The p75 neurotrophin receptor: multiple interactors and numerous functions. *Prog. Brain Res.*, **146**, 25–39.
10. Ibanez, C.F. and Simi, A. (2012) p75 neurotrophin receptor signaling in nervous system injury and degeneration: paradox and opportunity. *Trends Neurosci.*, **35**, 431–440.
11. Ma, Q., Yang, J., Li, T., Milner, T.A. and Hempstead, B.L. (2015) Selective reduction of striatal mature BDNF without induction of proBDNF in the zQ175 mouse model of Huntington's disease. *Neurobiol. Dis.*, **82**, 466–477.
12. Brito, V., Puigdellivol, M., Giralt, A., Del Toro, D., Alberch, J. and Gines, S. (2013) Imbalance of p75(NTR)/TrkB protein expression in Huntington's disease: implication for neuroprotective therapies. *Cell Death Dis.*, **4**, e595.
13. Fortress, A.M., Buhusi, M., Helke, K.L. and Granholm, A.C. (2011) Cholinergic Degeneration and Alterations in the TrkA and p75NTR Balance as a Result of Pro-NGF Injection into Aged Rats. *J. Aging Res.*, **2011**, 460543.
14. Yoon, S.O., Casaccia-Bonnefil, P., Carter, B. and Chao, M.V. (1998) Competitive signaling between TrkA and p75 nerve growth factor receptors determines cell survival. *J. Neurosci.*, **18**, 3273–3281.
15. Miguez, A., Garcia-Diaz Barriga, G., Brito, V., Straccia, M., Giralt, A., Gines, S., Canals, J.M. and Alberch, J. (2015) Fingolimod (FTY720) enhances hippocampal synaptic plasticity and memory in Huntington's disease by preventing p75NTR up-regulation and astrocyte-mediated inflammation. *Hum. Mol. Genet.*, **24**, 4958–4970.
16. Zuccato, C., Marullo, M., Conforti, P., MacDonald, M.E., Tartari, M. and Cattaneo, E. (2008) Systematic assessment of BDNF and its receptor levels in human cortices affected by Huntington's disease. *Brain Pathol.*, **18**, 225–238.
17. Plotkin, J.L., Day, M., Peterson, J.D., Xie, Z., Kress, G.J., Rafalovich, I., Kondapalli, J., Gertler, T.S., Flajolet, M., Greengard, P., *et al.* (2014) Impaired TrkB receptor signaling underlies corticostriatal dysfunction in Huntington's disease. *Neuron*, **83**, 178–188.
18. Simmons, D.A., Belichenko, N.P., Yang, T., Condon, C., Monbureau, M., Shamloo, M., Jing, D., Massa, S.M. and Longo, F.M. (2013) A small molecule TrkB ligand reduces motor impairment and neuropathology in R6/2 and BACHD mouse models of Huntington's disease. *J. Neurosci.*, **33**, 18712–18727.
19. Brito, V., Giralt, A., Enriquez-Barreto, L., Puigdellivol, M., Suelves, N., Zamora-Moratalla, A., Ballesteros, J.J., Martin, E.D., Dominguez-Iturza, N., Morales, M., *et al.* (2014) Neurotrophin receptor p75(NTR) mediates Huntington's disease-associated synaptic and memory dysfunction. *J. Clin. Invest.*, **124**, 4411–4428.
20. Bowles, K.R. and Jones, L. (2014) Kinase signalling in Huntington's disease. *J. Huntington's Dis.*, **3**, 89–123.
21. Longo, F.M. and Massa, S.M. (2008) Small molecule modulation of p75 neurotrophin receptor functions. *CNS Neurol. Disord. Drug Targets*, **7**, 63–70.
22. Longo, F.M. and Massa, S.M. (2013) Small-molecule modulation of neurotrophin receptors: a strategy for the treatment of neurological disease. *Nat. Rev. Drug Discov.*, **12**, 507–525.
23. Massa, S.M., Xie, Y., Yang, T., Harrington, A.W., Kim, M.L., Yoon, S.O., Kraemer, R., Moore, L.A., Hempstead, B.L. and Longo, F.M. (2006) Small, nonpeptide p75NTR ligands induce survival signaling and inhibit proNGF-induced death. *J. Neurosci.*, **26**, 5288–5300.
24. Yang, T., Knowles, J.K., Lu, Q., Zhang, H., Arancio, O., Moore, L.A., Chang, T., Wang, Q., Andreasson, K., Rajadas, J., *et al.* (2008) Small molecule, non-peptide p75 ligands inhibit Abeta-induced neurodegeneration and synaptic impairment. *PLoS One*, **3**, e3604.
25. Meeker, R.B., Poulton, W., Clary, G., Schriver, M. and Longo, F.M. (2016) Novel p75 neurotrophin receptor ligand stabilizes neuronal calcium, preserves mitochondrial movement and protects against HIV associated neuropathogenesis. *Exp. Neurol.*, **275 Pt 1**, 182–198.
26. Knowles, J.K., Rajadas, J., Nguyen, T.V., Yang, T., LeMieux, M.C., Vander Griend, L., Ishikawa, C., Massa, S.M., Wyss-Coray, T. and Longo, F.M. (2009) The p75 neurotrophin receptor promotes amyloid-beta(1-42)-induced neuritic dystrophy in vitro and in vivo. *J. Neurosci.*, **29**, 10627–10637.
27. Meeker, R.B., Poulton, W., Feng, W.H., Hudson, L. and Longo, F.M. (2012) Suppression of Immunodeficiency Virus-Associated Neural Damage by the p75 Neurotrophin Receptor Ligand, LM11A-31, in an In Vitro Feline Model. *J. Neuroimmune. Pharmacol.*, **7**, 388–400.
28. James, S.E., Burden, H., Burgess, R., Xie, Y., Yang, T., Massa, S.M., Longo, F.M. and Lu, Q. (2008) Anti-cancer drug induced neurotoxicity and identification of Rho pathway signaling modulators as potential neuroprotectants. *Neurotoxicology*, **29**, 605–612.
29. Friesland, A., Weng, Z., Duenas, M., Massa, S.M., Longo, F.M. and Lu, Q. (2014) Amelioration of cisplatin-induced experimental peripheral neuropathy by a small molecule targeting p75 NTR. *Neurotoxicology*, **45**, 81–90.
30. Shi, J., Longo, F.M. and Massa, S.M. (2013) A small molecule p75(NTR) ligand protects neurogenesis after traumatic brain injury. *Stem Cells*, **31**, 2561–2574.
31. Tep, C., Lim, T.H., Ko, P.O., Getahun, S., Ryu, J.C., Goettl, V.M., Massa, S.M., Basso, M., Longo, F.M. and Yoon, S.O.

(2013) Oral administration of a small molecule targeted to block proNGF binding to p75 promotes myelin sparing and functional recovery after spinal cord injury. *J. Neurosci.*, **33**, 397–410.
32. Knowles, J.K., Simmons, D.A., Nguyen, T.V., Vander Griend, L., Xie, Y., Zhang, H., Yang, T., Pollak, J., Chang, T., Arancio, O., *et al.* (2013) A small molecule p75NTR ligand prevents cognitive deficits and neurite degeneration in an Alzheimer's mouse model. *Neurobiol. Aging*, **34**, 2052–2063.
33. Nguyen, T.V., Shen, L., Vander Griend, L., Quach, L.N., Belichenko, N.P., Saw, N., Yang, T., Shamloo, M., Wyss-Coray, T., Massa, S.M., *et al.* (2014) Small molecule p75NTR ligands reduce pathological phosphorylation and misfolding of tau, inflammatory changes, cholinergic degeneration, and cognitive deficits in AbetaPP(L/S) transgenic mice. *J. Alzheimer's Dis.*, **42**, 459–483.
34. Simmons, D.A., Knowles, J.K., Belichenko, N.P., Banerjee, G., Finkle, C., Massa, S.M. and Longo, F.M. (2014) A small molecule p75NTR ligand, LM11A-31, reverses cholinergic neurite dystrophy in Alzheimer's disease mouse models with mid- to late-stage disease progression. *PLoS One*, **9**, e102136.
35. Kanning, K.C., Hudson, M., Amieux, P.S., Wiley, J.C., Bothwell, M. and Schecterson, L.C. (2003) Proteolytic processing of the p75 neurotrophin receptor and two homologs generates C-terminal fragments with signaling capability. *J. Neurosci.*, **23**, 5425–5436.
36. Ceni, C., Kommaddi, R.P., Thomas, R., Vereker, E., Liu, X., McPherson, P.S., Ritter, B. and Barker, P.A. (2010) The p75NTR intracellular domain generated by neurotrophin-induced receptor cleavage potentiates Trk signaling. *J. Cell Sci.*, **123**, 2299–2307.
37. Skeldal, S., Matusica, D., Nykjaer, A. and Coulson, E.J. (2011) Proteolytic processing of the p75 neurotrophin receptor: A prerequisite for signalling?: Neuronal life, growth and death signalling are crucially regulated by intra-membrane proteolysis and trafficking of p75(NTR). *Bioessays*, **33**, 614–625.
38. Vicario, A., Kisiswa, L., Tann, J.Y., Kelly, C.E. and Ibanez, C.F. (2015) Neuron-type-specific signaling by the p75NTR death receptor is regulated by differential proteolytic cleavage. *J. Cell Sci.*, **128**, 1507–1517.
39. Roux, P.P., Bhakar, A.L., Kennedy, T.E. and Barker, P.A. (2001) The p75 neurotrophin receptor activates Akt (protein kinase B) through a phosphatidylinositol 3-kinase-dependent pathway. *J. Biol. Chem.*, **276**, 23097–23104.
40. Colin, E., Regulier, E., Perrin, V., Durr, A., Brice, A., Aebischer, P., Deglon, N., Humbert, S. and Saudou, F. (2005) Akt is altered in an animal model of Huntington's disease and in patients. *Eur. J. Neurosci.*, **21**, 1478–1488.
41. Fan, J., Gladding, C.M., Wang, L., Zhang, L.Y., Kaufman, A.M., Milnerwood, A.J. and Raymond, L.A. (2012) P38 MAPK is involved in enhanced NMDA receptor-dependent excitotoxicity in YAC transgenic mouse model of Huntington disease. *Neurobiol. Dis.*, **45**, 999–1009.
42. Gianfriddo, M., Melani, A., Turchi, D., Giovannini, M.G. and Pedata, F. (2004) Adenosine and glutamate extracellular concentrations and mitogen-activated protein kinases in the striatum of Huntington transgenic mice. Selective antagonism of adenosine A2A receptors reduces transmitter outflow. *Neurobiol. Dis.*, **17**, 77–88.
43. Taylor, D.M., Moser, R., Regulier, E., Breuillaud, L., Dixon, M., Beesen, A.A., Elliston, L., Silva Santos Mde, F., Kim, J., Jones, L., *et al.* (2013) MAP kinase phosphatase 1 (MKP-1/DUSP1) is neuroprotective in Huntington's disease via additive effects of JNK and p38 inhibition. *J. Neurosci.*, **33**, 2313–2325.
44. Mattson, M.P. and Meffert, M.K. (2006) Roles for NF-kappaB in nerve cell survival, plasticity, and disease. *Cell Death Differ.*, **13**, 852–860.
45. Khoshnan, A., Ko, J., Watkin, E.E., Paige, L.A., Reinhart, P.H. and Patterson, P.H. (2004) Activation of the IkappaB kinase complex and nuclear factor-kappaB contributes to mutant huntingtin neurotoxicity. *J. Neurosci.*, **24**, 7999–8008.
46. Trager, U., Andre, R., Lahiri, N., Magnusson-Lind, A., Weiss, A., Grueninger, S., McKinnon, C., Sirinathsinghji, E., Kahlon, S., Pfister, E.L., *et al.* (2014) HTT-lowering reverses Huntington's disease immune dysfunction caused by NFkappaB pathway dysregulation. *Brain*, **137**, 819–833.
47. Hayden, M.S. and Ghosh, S. (2012) NF-kappaB, the first quarter-century: remarkable progress and outstanding questions. *Genes Dev.*, **26**, 203–234.
48. Huxford, T., Huang, D.B., Malek, S. and Ghosh, G. (1998) The crystal structure of the IkappaBalpha/NF-kappaB complex reveals mechanisms of NF-kappaB inactivation. *Cell*, **95**, 759–770.
49. Khoshnan, A. and Patterson, P.H. (2011) The role of IkappaB kinase complex in the neurobiology of Huntington's disease. *Neurobiol. Dis.*, **43**, 305–311.
50. Yamashita, T., Tucker, K.L. and Barde, Y.A. (1999) Neurotrophin binding to the p75 receptor modulates Rho activity and axonal outgrowth. *Neuron*, **24**, 585–593.
51. Yamashita, T. and Tohyama, M. (2003) The p75 receptor acts as a displacement factor that releases Rho from Rho-GDI. *Nat. Neurosci.*, **6**, 461–467.
52. Bauer, P.O., Wong, H.K., Oyama, F., Goswami, A., Okuno, M., Kino, Y., Miyazaki, H. and Nukina, N. (2009) Inhibition of Rho kinases enhances the degradation of mutant huntingtin. *J. Biol. Chem.*, **284**, 13153–13164.
53. Li, M., Huang, Y., Ma, A.A., Lin, E. and Diamond, M.I. (2009) Y-27632 improves rotarod performance and reduces huntingtin levels in R6/2 mice. *Neurobiol. Dis.*, **36**, 413–420.
54. Narayanan, K.L., Chopra, V., Rosas, H.D., Malarick, K. and Hersch, S. (2015) Rho Kinase Pathway Alterations in the Brain and Leukocytes in Huntington's Disease. *Mol. Neurobiol.*, **53**, 2132–2140.
55. Song, W., Volosin, M., Cragnolini, A.B., Hempstead, B.L. and Friedman, W.J. (2010) ProNGF induces PTEN via p75NTR to suppress Trk-mediated survival signaling in brain neurons. *J. Neurosci.*, **30**, 15608–15615.
56. Yang, S. and Kim, H.M. (2012) The RhoA-ROCK-PTEN pathway as a molecular switch for anchorage dependent cell behavior. *Biomaterials*, **33**, 2902–2915.
57. Koth, A.P., Oliveira, B.R., Parfitt, G.M., Buonocore Jde, Q. and Barros, D.M. (2014) Participation of group I p21-activated kinases in neuroplasticity. *J. Physiol. Paris*, **108**, 270–277.
58. Rex, C.S., Chen, L.Y., Sharma, A., Liu, J., Babayan, A.H., Gall, C.M. and Lynch, G. (2009) Different Rho GTPase-dependent signaling pathways initiate sequential steps in the consolidation of long-term potentiation. *J. Cell Biol.*, **186**, 85–97.
59. Schurmann, A., Mooney, A.F., Sanders, L.C., Sells, M.A., Wang, H.G., Reed, J.C. and Bokoch, G.M. (2000) p21-activated kinase 1 phosphorylates the death agonist bad and protects cells from apoptosis. *Mol. Cell. Biol.*, **20**, 453–461.
60. DiFiglia, M., Sapp, E., Chase, K., Davies, S., Bates, G., Vonsattel, J. and Aronin, N. (1997) Aggregation of huntingtin in neuronal intranuclear inclusions and dystrophic neurites in brain. *Science*, **277**, 1990–1993.

61. Zuccato, C., Valenza, M. and Cattaneo, E. (2010) Molecular mechanisms and potential therapeutical targets in Huntington's disease. *Physiol.Rev.*, **90**, 905–981.
62. Pouladi, M.A., Morton, A.J. and Hayden, M.R. (2013) Choosing an animal model for the study of Huntington's disease. *Nat. Rev. Neurosci.*, **14**, 708–721.
63. Gray, M., Shirasaki, D.I., Cepeda, C., Andre, V.M., Wilburn, B., Lu, X.H., Tao, J., Yamazaki, I., Li, S.H., Sun, Y.E., *et al.* (2008) Full-length human mutant huntingtin with a stable polyglutamine repeat can elicit progressive and selective neuropathogenesis in BACHD mice. *J. Neurosci.*, **28**, 6182–6195.
64. Pouladi, M.A., Stanek, L.M., Xie, Y., Franciosi, S., Southwell, A.L., Deng, Y., Butland, S., Zhang, W., Cheng, S.H., Shihabuddin, L.S., *et al.* (2012) Marked differences in neurochemistry and aggregates despite similar behavioural and neuropathological features of Huntington disease in the full-length BACHD and YAC128 mice. *Hum. Mol.Genet.*, **21**, 2219–2232.
65. Bibb, J.A., Yan, Z., Svenningsson, P., Snyder, G.L., Pieribone, V.A., Horiuchi, A., Nairn, A.C., Messer, A. and Greengard, P. (2000) Severe deficiencies in dopamine signaling in presymptomatic Huntington's disease mice. *Proc. Natl. Acad. Sci. U. S. A*, **97**, 6809–6814.
66. Bogush, A., Pedrini, S., Pelta-Heller, J., Chan, T., Yang, Q., Mao, Z., Sluzas, E., Gieringer, T. and Ehrlich, M.E. (2007) AKT and CDK5/p35 mediate brain-derived neurotrophic factor induction of DARPP-32 in medium size spiny neurons in vitro. *J. Biol. Chem.*, **282**, 7352–7359.
67. van Dellen, A., Welch, J., Dixon, R.M., Cordery, P., York, D., Styles, P., Blakemore, C. and Hannan, A.J. (2000) N-Acetylaspartate and DARPP-32 levels decrease in the corpus striatum of Huntington's disease mice. *Neuroreport*, **11**, 3751–3757.
68. Mangiarini, L., Sathasivam, K., Seller, M., Cozens, B., Harper, A., Hetherington, C., Lawton, M., Trottier, Y., Lehrach, H., Davies, S., *et al.* (1996) Exon 1 of the HD gene with an expanded CAG repeat is sufficient to cause a progressive neurological phenotype in transgenic mice. *Cell*, **87**, 493–506.
69. Ferrante, R.J., Kowall, N.W., Beal, M.F., Richardson, E.P., Jr., Bird, E.D. and Martin, J.B. (1985) Selective sparing of a class of striatal neurons in Huntington's disease. *Science*, **230**, 561–563.
70. Ferrante, R.J., Beal, M.F., Kowall, N.W., Richardson, E.P., Jr. and Martin, J.B. (1987) Sparing of acetylcholinesterase-containing striatal neurons in Huntington's disease. *Brain Res.*, **411**, 162–166.
71. Cicchetti, F., Prensa, L., Wu, Y. and Parent, A. (2000) Chemical anatomy of striatal interneurons in normal individuals and in patients with Huntington's disease. *Brain Res. Brain Res. Rev.*, **34**, 80–101.
72. Holley, S.M., Joshi, P.R., Parievsky, A., Galvan, L., Chen, J.Y., Fisher, Y.E., Huynh, M.N., Cepeda, C. and Levine, M.S. (2015) Enhanced GABAergic Inputs Contribute to Functional Alterations of Cholinergic Interneurons in the R6/2 Mouse Model of Huntington's Disease. *eNeuro*, **2**, pii: e0008.
73. Deng, Y.P. and Reiner, A. (2016) Cholinergic interneurons in the Q140 knock-in mouse model of Huntington's disease: Reductions in dendritic branching and thalamostriatal input. *J Comp. Neurol.*, Epub ahead of print. doi: 10.1002/cne.24013.
74. Meade, C., Deng, Y., Fusco, F., Del Mar, N., Hersch, S., Goldowitz, D. and Reiner, A. (2002) Cellular localization and development of neuronal intranuclear inclusions in striatal and cortical neurons in R6/2 transgenic mice. *J. Comp. Neurol.*, **449**, 241–269.
75. Kosinski, C.M., Cha, J.H., Young, A.B., Mangiarini, L., Bates, G., Schiefer, J. and Schwarz, M. (1999) Intranuclear inclusions in subtypes of striatal neurons in Huntington's disease transgenic mice. *Neuroreport*, **10**, 3891–3896.
76. Farrar, A.M., Callahan, J.W. and Abercrombie, E.D. (2011) Reduced striatal acetylcholine efflux in the R6/2 mouse model of Huntington's disease: an examination of the role of altered inhibitory and excitatory mechanisms. *Exp. Neurol.*, **232**, 119–125.
77. Smith, R., Chung, H., Rundquist, S., Maat-Schieman, M.L., Colgan, L., Englund, E., Liu, Y.J., Roos, R.A., Faull, R.L., Brundin, P., *et al.* (2006) Cholinergic neuronal defect without cell loss in Huntington's disease. *Hum. Mol. Genet.*, **15**, 3119–3131.
78. Vetter, J.M., Jehle, T., Heinemeyer, J., Franz, P., Behrens, P.F., Jackisch, R., Landwehrmeyer, G.B. and Feuerstein, T.J. (2003) Mice transgenic for exon 1 of Huntington's disease: properties of cholinergic and dopaminergic pre-synaptic function in the striatum. *J. Neurochem.*, **85**, 1054–1063.
79. Picconi, B., Passino, E., Sgobio, C., Bonsi, P., Barone, I., Ghiglieri, V., Pisani, A., Bernardi, G., Ammassari-Teule, M. and Calabresi, P. (2006) Plastic and behavioral abnormalities in experimental Huntington's disease: a crucial role for cholinergic interneurons. *Neurobiol. Dis.*, **22**, 143–152.
80. Jones, L. and Hughes, A. (2011) Pathogenic mechanisms in Huntington's disease. *Int. Rev. Neurobiol.*, **98**, 373–418.
81. Parsons, M.P. and Raymond, L.A. (2014) Extrasynaptic NMDA receptor involvement in central nervous system disorders. *Neuron*, **82**, 279–293.
82. Imai, Y., Ibata, I., Ito, D., Ohsawa, K. and Kohsaka, S. (1996) A novel gene iba1 in the major histocompatibility complex class III region encoding an EF hand protein expressed in a monocytic lineage. *Biochem. Biophys. Res. Commun.*, **224**, 855–862.
83. Ito, D., Imai, Y., Ohsawa, K., Nakajima, K., Fukuuchi, Y. and Kohsaka, S. (1998) Microglia-specific localisation of a novel calcium binding protein, Iba1. *Brain Res. Mol. Brain Res.*, **57**, 1–9.
84. Ridley, A., Paterson, H., Johnston, C., Diekmann, D. and Hall, A. (1992) The small GTP-binding protein rac regulates growth factor-induced membrane ruffling. *Cell*, **70**, 401–410.
85. Simmons, D.A., Casale, M., Alcon, B., Pham, N., Narayan, N. and Lynch, G. (2007) Ferritin accumulation in dystrophic microglia is an early event in the development of Huntington's disease. *Glia*, **55**, 1074–1084.
86. Wacker, J.L., Huang, S.Y., Steele, A.D., Aron, R., Lotz, G.P., Nguyen, Q., Giorgini, F., Roberson, E.D., Lindquist, S., Masliah, E., *et al.* (2009) Loss of Hsp70 exacerbates pathogenesis but not levels of fibrillar aggregates in a mouse model of Huntington's disease. *J. Neurosci.*, **29**, 9104–9114.
87. Franciosi, S., Ryu, J.K., Shim, Y., Hill, A., Connolly, C., Hayden, M.R., McLarnon, J.G. and Leavitt, B.R. (2012) Age-dependent neurovascular abnormalities and altered microglial morphology in the YAC128 mouse model of Huntington disease. *Neurobiol. Dis.*, **45**, 438–449.
88. Mantovani, S., Gordon, R., Li, R., Christie, D.C., Kumar, V. and Woodruff, T.M. (2016) Motor deficits associated with Huntington's disease occur in the absence of striatal degeneration in BACHD transgenic mice. *Hum. Mol. Genet.*, **25**, 1780–1791.

89. Crotti, A. and Glass, C.K. (2015) The choreography of neuroinflammation in Huntington's disease. *Trends Immunol.*, **36**, 364–373.
90. Ferrante, R.J., Kowall, N.W. and Richardson, E.P. Jr. (1991) Proliferative and degenerative changes in striatal spiny neurons in Huntington's disease: a combined study using the section-Golgi method and calbindin D28k immunocytochemistry. *J. Neurosci.*, **11**, 3877–3887.
91. Graveland, G., Williams, R. and DiFiglia, M. (1985) Evidence for degenerative and regenerative changes in neostriatal spiny neurons in Huntington's disease. *Science*, **227**, 770–773.
92. Heck, N., Betuing, S., Vanhoutte, P. and Caboche, J. (2012) A deconvolution method to improve automated 3D-analysis of dendritic spines: application to a mouse model of Huntington's disease. *Brain Struct. Funct.*, **217**, 421–434.
93. Klapstein, G.J., Fisher, R.S., Zanjani, H., Cepeda, C., Jokel, E.S., Chesselet, M.F. and Levine, M.S. (2001) Electrophysiological and morphological changes in striatal spiny neurons in R6/2 Huntington's disease transgenic mice. *J. Neurophysiol.*, **86**, 2667–2677.
94. Rocher, A.B., Gubellini, P., Merienne, N., Boussicault, L., Petit, F., Gipchtein, P., Jan, C., Hantraye, P., Brouillet, E. and Bonvento, G. (2016) Synaptic scaling up in medium spiny neurons of aged BACHD mice: A slow-progression model of Huntington's disease. *Neurobiol. Dis.*, **86**, 131–139.
95. Dougherty, K.D. and Milner, T.A. (1999) p75NTR immunoreactivity in the rat dentate gyrus is mostly within presynaptic profiles but is also found in some astrocytic and postsynaptic profiles. *J. Comp. Neurol.*, **407**, 77–91.
96. Woo, N.H., Teng, H.K., Siao, C.J., Chiaruttini, C., Pang, P.T., Milner, T.A., Hempstead, B.L. and Lu, B. (2005) Activation of p75NTR by proBDNF facilitates hippocampal long-term depression. *Nat. Neurosci.*, **8**, 1069–1077.
97. Zagrebelsky, M., Holz, A., Dechant, G., Barde, Y.A., Bonhoeffer, T. and Korte, M. (2005) The p75 neurotrophin receptor negatively modulates dendrite complexity and spine density in hippocampal neurons. *J. Neurosci.*, **25**, 9989–9999.
98. Bolivar, V.J., Manley, K. and Messer, A. (2003) Exploratory activity and fear conditioning abnormalities develop early in R6/2 Huntington's disease transgenic mice. *Behav. Neurosci.*, **117**, 1233–1242.
99. Carter, R., Lione, L., Humby, T., Mangiarini, L., Mahal, A., Bates, G., Dunnett, S. and Morton, A. (1999) Characterization of progressive motor deficits in mice transgenic for the human Huntington's disease mutation. *J. Neurosci.*, **19**, 3248–3257.
100. Hickey, M.A., Gallant, K., Gross, G.G., Levine, M.S. and Chesselet, M.F. (2005) Early behavioral deficits in R6/2 mice suitable for use in preclinical drug testing. *Neurobiol. Dis.*, **20**, 1–11.
101. Menalled, L., El-Khodor, B.F., Patry, M., Suarez-Farinas, M., Orenstein, S.J., Zahasky, B., Leahy, C., Wheeler, V., Yang, X.W., MacDonald, M., *et al.* (2009) Systematic behavioral evaluation of Huntington's disease transgenic and knock-in mouse models. *Neurobiol. Dis.*, **35**, 319–336.
102. Casaca-Carreira, J., Temel, Y., van Zelst, M. and Jahanshahi, A. (2015) Coexistence of Gait Disturbances and Chorea in Experimental Huntington's Disease. *Behav. Neurol.*, **2015**, 970204.
103. Abada, Y.S., Schreiber, R. and Ellenbroek, B. (2012) Motor, emotional and cognitive deficits in adult BACHD mice: A model for Huntington's disease. *Behav. Brain Res.*, **238**, 243–251.
104. Grimbergen, Y.A., Knol, M.J., Bloem, B.R., Kremer, B.P., Roos, R.A. and Munneke, M. (2008) Falls and gait disturbances in Huntington's disease. *Mov. Disord.*, **23**, 970–976.
105. Koller, W.C. and Trimble, J. (1985) The gait abnormality of Huntington's disease. *Neurology*, **35**, 1450–1454.
106. Shu, Y.H., Lu, X.M., Wei, J.X., Xiao, L. and Wang, Y.T. (2015) Update on the role of p75NTR in neurological disorders: A novel therapeutic target. *Biomed. Pharmacother.*, **76**, 17–23.
107. Dechant, G. and Barde, Y.A. (2002) The neurotrophin receptor p75(NTR): novel functions and implications for diseases of the nervous system. *Nat. Neurosci.*, **5**, 1131–1136.
108. Meeker, R.B. and Williams, K.S. (2015) The p75 neurotrophin receptor: at the crossroad of neural repair and death. *Neural Regen. Res.*, **10**, 721–725.
109. Frade, J.M. (2005) Nuclear translocation of the p75 neurotrophin receptor cytoplasmic domain in response to neurotrophin binding. *J. Neurosci.*, **25**, 1407–1411.
110. Jung, K.M., Tan, S., Landman, N., Petrova, K., Murray, S., Lewis, R., Kim, P.K., Kim, D.S., Ryu, S.H., Chao, M.V., *et al.* (2003) Regulated intramembrane proteolysis of the p75 neurotrophin receptor modulates its association with the TrkA receptor. *J. Biol. Chem.*, **278**, 42161–42169.
111. Humbert, S., Bryson, E.A., Cordelieres, F.P., Connors, N.C., Datta, S.R., Finkbeiner, S., Greenberg, M.E. and Saudou, F. (2002) The IGF-1/Akt pathway is neuroprotective in Huntington's disease and involves Huntingtin phosphorylation by Akt. *Dev. Cell*, **2**, 831–837.
112. Rangone, H., Pardo, R., Colin, E., Girault, J.A., Saudou, F. and Humbert, S. (2005) Phosphorylation of arfaptin 2 at Ser260 by Akt Inhibits PolyQ-huntingtin-induced toxicity by rescuing proteasome impairment. *J. Biol. Chem.*, **280**, 22021–22028.
113. Zala, D., Colin, E., Rangone, H., Liot, G., Humbert, S. and Saudou, F. (2008) Phosphorylation of mutant huntingtin at S421 restores anterograde and retrograde transport in neurons. *Hum. Mol. Genet.*, **17**, 3837–3846.
114. Hensel, N., Rademacher, S. and Claus, P. (2015) Chatting with the neighbors: crosstalk between Rho-kinase (ROCK) and other signaling pathways for treatment of neurological disorders. *Front. Neurosci.*, **9**, 198.
115. Bauer, P.O. and Nukina, N. (2009) Enhanced degradation of mutant huntingtin by rho kinase inhibition is mediated through activation of proteasome and macroautophagy. *Autophagy*, **5**, 747–748.
116. Shao, J., Welch, W.J., Diprospero, N.A. and Diamond, M.I. (2008) Phosphorylation of profilin by ROCK1 regulates polyglutamine aggregation. *Mol. Cell. Cell. Biol.*, **28**, 5196–5208.
117. Perrin, V., Dufour, N., Raoul, C., Hassig, R., Brouillet, E., Aebischer, P., Luthi-Carter, R. and Deglon, N. (2009) Implication of the JNK pathway in a rat model of Huntington's disease. *Exp. Neurol.*, **215**, 191–200.
118. Govek, E., Newey, S. and Van Aelst, L. (2005) The role of the Rho GTPases in neuronal development. *Genes Dev.*, **19**, 1–49.
119. Nakayama, A.Y., Harms, M.B. and Luo, L. (2000) Small GTPases Rac and Rho in the maintenance of dendritic spines and branches in hippocampal pyramidal neurons. *J. Neurosci.*, **20**, 5329–5338.
120. Zhang, H., Petit, G.H., Gaughwin, P.M., Hansen, C., Ranganathan, S., Zuo, X., Smith, R., Roybon, L., Brundin, P., Mobley, W.C., *et al.* (2013) NGF rescues hippocampal cholinergic neuronal markers, restores neurogenesis, and

improves the spatial working memory in a mouse model of Huntington's Disease. *J. Huntington's Dis.*, **2**, 69–82.
121. Chopra, V., Fox, J.H., Lieberman, G., Dorsey, K., Matson, W., Waldmeier, P., Housman, D.E., Kazantsev, A., Young, A.B. and Hersch, S. (2007) A small-molecule therapeutic lead for Huntington's disease: preclinical pharmacology and efficacy of C2-8 in the R6/2 transgenic mouse. *Proc. Natl Acad. Sci. U. S. A*, **104**, 16685–16689.
122. Dedeoglu, A., Kubilus, J.K., Jeitner, T.M., Matson, S.A., Bogdanov, M., Kowall, N.W., Matson, W.R., Cooper, A.J., Ratan, R.R., Beal, M.F., *et al.* (2002) Therapeutic effects of cystamine in a murine model of Huntington's disease. *J. Neurosci.*, **22**, 8942–8950.
123. Duan, W., Guo, Z., Jiang, H., Ware, M., Li, X. and Mattson, M. (2003) Dietary restriction normalizes glucose metabolism and BDNF levels, slows disease progression, and increases survival in huntingtin mutant mice. *Proc. Natl. Acad. Sci. U. S. A*, **100**, 2911–2916.
124. Ferrante, R.J., Andreassen, O.A., Dedeoglu, A., Ferrante, K.L., Jenkins, B.G., Hersch, S.M. and Beal, M.F. (2002) Therapeutic effects of coenzyme Q10 and remacemide in transgenic mouse models of Huntington's disease. *J. Neurosci.*, **22**, 1592–1599.
125. Yamamoto, A., Lucas, J.J. and Hen, R. (2000) Reversal of neuropathology and motor dysfunction in a conditional model of Huntington's disease. *Cell*, **101**, 57–66.
126. Bokoch, G.M. (2003) Biology of the p21-activated kinases. *Annu. Rev. Biochem.*, **72**, 743–781.
127. Penzes, P. and Cahill, M.E. (2012) Deconstructing signal transduction pathways that regulate the actin cytoskeleton in dendritic spines. *Cytoskeleton*, **69**, 426–441.
128. Penzes, P. and Rafalovich, I. (2012) Regulation of the actin cytoskeleton in dendritic spines. *Adv. Exp. Med.Biol.*, **970**, 81–95.
129. Majumdar, D., Nebhan, C.A., Hu, L., Anderson, B. and Webb, D.J. (2011) An APPL1/Akt signaling complex regulates dendritic spine and synapse formation in hippocampal neurons. *Mol. Cell. Neurosci.*, **46**, 633–644.
130. Tashiro, A. and Yuste, R. (2008) Role of Rho GTPases in the morphogenesis and motility of dendritic spines. *Methods Enzymol.*, **439**, 285–302.
131. Hong, S.L., Cossyleon, D., Hussain, W.A., Walker, L.J., Barton, S.J. and Rebec, G.V. (2012) Dysfunctional behavioral modulation of corticostriatal communication in the R6/2 mouse model of Huntington's disease. *PLoS One*, **7**, e47026.
132. Aosaki, T., Graybiel, A.M. and Kimura, M. (1994) Effect of the nigrostriatal dopamine system on acquired neural responses in the striatum of behaving monkeys. *Science*, **265**, 412–415.
133. Chen, J.Y., Wang, E.A., Cepeda, C. and Levine, M.S. (2013) Dopamine imbalance in Huntington's disease: a mechanism for the lack of behavioral flexibility. *Front. Neurosci.*, **7**, 114.
134. Lawrence, A., Hodges, J., Rosser, A., Kershaw, A., French-Constant, C., Rubinsztein, D. and Robbins, T. and BJ, S. (1998) Evidence for specific cognitive deficits in preclinical Huntington's disease. *Brain Pathol.*, **121**, 1329–1341.
135. Lawrence, A.D., Sahakian, B.J., Hodges, J.R., Rosser, A.E., Lange, K.W. and Robbins, T.W. (1996) Executive and mnemonic functions in early Huntington's disease. *Brain*, **119**, 1633–1645.
136. Rao, A.K., Muratori, L., Louis, E.D., Moskowitz, C.B. and Marder, K.S. (2008) Spectrum of gait impairments in presymptomatic and symptomatic Huntington's disease. *Mov. Disord.*, **23**, 1100–1107.
137. Bylsma, F.W., Rothlind, J., Hall, M.R., Folstein, S.E. and Brandt, J. (1993) Assessment of adaptive functioning in Huntington's disease. *Mov. Disord.*, **8**, 183–190.
138. Marder, K., Zhao, H., Myers, R.H., Cudkowicz, M., Kayson, E., Kieburtz, K., Orme, C., Paulsen, J., Penney, J.B., Jr., Siemers, E., *et al.* (2000) Rate of functional decline in Huntington's disease. Huntington Study Group. *Neurology*, **54**, 452–458.
139. Wheelock, V.L., Tempkin, T., Marder, K., Nance, M., Myers, R.H., Zhao, H., Kayson, E., Orme, C., Shoulson, I. and Huntington Study, G. (2003) Predictors of nursing home placement in Huntington disease. *Neurology*, **60**, 998–1001.
140. Simmons, D.A., Mehta, R.A., Lauterborn, J.C., Gall, C.M. and Lynch, G. (2011) Brief ampakine treatments slow the progression of Huntington's disease phenotypes in R6/2 mice. *Neurobiol. Dis.*, **41**, 436–444.
141. Balci, F., Oakeshott, S., Shamy, J.L., El-Khodor, B.F., Filippov, I., Mushlin, R., Port, R., Connor, D., Paintdakhi, A., Menalled, L., *et al.* (2013) High-Throughput Automated Phenotyping of Two Genetic Mouse Models of Huntington's Disease. *PLoS Currents*, **5**, doi: 10.1371/currents.hd.124aa0d16753f88215776fba102ceb29.
142. Rudenko, O., Tkach, V., Berezin, V. and Bock, E. (2009) Detection of early behavioral markers of Huntington's disease in R6/2 mice employing an automated social home cage. *Behav. Brain Res.*, **203**, 188–199.
143. Franklin, K. and Paxinos, G. (2008) *The Mouse Brain in Stereotaxic Coordinates*. Elsevier Inc., New York.
144. Lerner, R.P., Trejo Martinez Ldel, C., Zhu, C., Chesselet, M.F. and Hickey, M.A. (2012) Striatal atrophy and dendritic alterations in a knock-in mouse model of Huntington's disease. *Brain Res. Bull.*, **87**, 571–578.
145. Bourne, J.N. and Harris, K.M. (2008) Balancing structure and function at hippocampal dendritic spines. *Annu. Rev. Neurosci.*, **31**, 47–67.